



**HAL**  
open science

## **Thrombosis in the Coronary Microvasculature Impairs Cardiac Relaxation and Induces Diastolic Dysfunction**

Paul Rouault, Sarah Guimbal, Lauriane Cornuault, Célia Bourguignon, Ninon Foussard, Philippe Alzieu, Frank Choveau, David Benoist, Candice Chapouly, Alain-Pierre Gadeau, et al.

### ► To cite this version:

Paul Rouault, Sarah Guimbal, Lauriane Cornuault, Célia Bourguignon, Ninon Foussard, et al.. Thrombosis in the Coronary Microvasculature Impairs Cardiac Relaxation and Induces Diastolic Dysfunction. *Arteriosclerosis, Thrombosis, and Vascular Biology*, 2023, 44 (1), pp.e1-e18. 10.1161/ATVBAHA.123.320040 . inserm-04322686

**HAL Id: inserm-04322686**

**<https://inserm.hal.science/inserm-04322686v1>**

Submitted on 5 Dec 2023

**HAL** is a multi-disciplinary open access archive for the deposit and dissemination of scientific research documents, whether they are published or not. The documents may come from teaching and research institutions in France or abroad, or from public or private research centers.

L'archive ouverte pluridisciplinaire **HAL**, est destinée au dépôt et à la diffusion de documents scientifiques de niveau recherche, publiés ou non, émanant des établissements d'enseignement et de recherche français ou étrangers, des laboratoires publics ou privés.

**Full title**

Thrombosis in the coronary microvasculature impairs cardiac relaxation and induces diastolic dysfunction

**Authors' names, academic degrees, and affiliations**

Paul Rouault, MS<sup>1\*</sup>, Sarah Guimbal, PhD<sup>1\*</sup>, Lauriane Cornuault, PhD<sup>1</sup>, Célia Bourguignon, MS<sup>1</sup>, Ninon Foussard MD<sup>1</sup>, Philippe Alzieu, BS<sup>1</sup>, Frank Choveau, PhD<sup>2</sup>, David Benoist, PhD<sup>2</sup>, Candice Chapouly, PharmD, PhD<sup>1</sup> Alain-Pierre Gadeau, PhD<sup>1</sup>, Thierry Couffinhal, MD, PhD<sup>1</sup>, and Marie-Ange Renault, PhD<sup>1</sup>

\* These authors contributed equally to this work

<sup>1</sup> Univ. Bordeaux, Inserm, Biology of Cardiovascular Diseases, U1034, F-33600 Pessac, France

<sup>2</sup> Univ. Bordeaux, INSERM, CRCTB, U 1045, IHU Liryc, F-33000 Bordeaux, France

**Short title**

Thrombosis promotes HFpEF

**Name, email address, and complete address of corresponding author**

Marie-Ange Renault

marie-ange.renault@inserm.fr

Inserm U1034

1, avenue de Magellan

Entrée par l'Hôpital Haut-Lévêque

33604 Pessac

France

Tel: (33) 5 57 89 19 79

**Total word count:** 8234 words

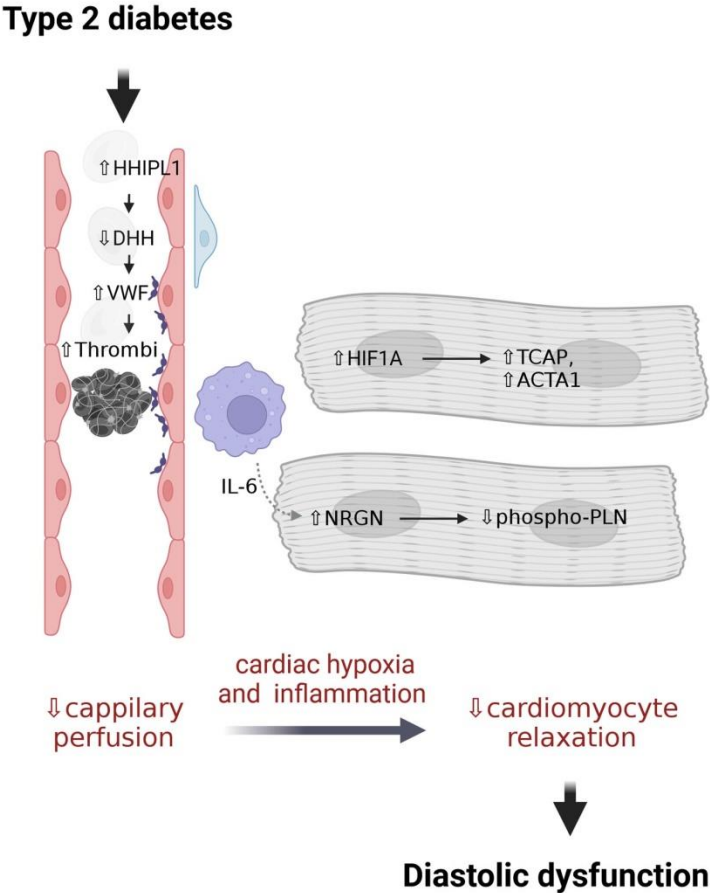
## ABSTRACT

**Background:** Heart Failure with Preserved Ejection Fraction (HFpEF) is proposed to be caused by endothelial dysfunction in cardiac microvessels. Our goal was to identify molecular and cellular mechanisms underlying the development of cardiac microvessel disease and diastolic dysfunction in the setting of type 2 diabetes. **Methods:** We used Leptin receptor-deficient (*Lepr<sup>db/db</sup>*) female mice as a model of type 2 diabetes and HFpEF and identified Hedgehog interacting protein-like 1 (Hhip1) which encodes for a decoy receptor for Hedgehog (HH) ligands as a gene upregulated in the cardiac vascular fraction of diseased mice. **Results:** We then used Desert Hedgehog (Dhh) deficient mice to investigate the functional consequences of impaired HH signaling in the adult heart. We found that Dhh deficient mice displayed increased end-diastolic pressure while left ventricular ejection fraction was comparable to that of control mice. This phenotype was associated with a reduced exercise tolerance in the treadmill test suggesting that Dhh deficient mice do present heart failure. At molecular and cellular levels, impaired cardiac relaxation in *Dhh<sup>ECKO</sup>* mice was associated with a significantly decreased phospholamban phosphorylation on Thr17 and an alteration of sarcomeric shortening ex-vivo. Besides, as expected, Dhh deficient mice exhibited phenotypic changes in their cardiac microvessels including a prominent pro-thrombotic phenotype. Importantly, aspirin therapy prevented the occurrence of both diastolic dysfunction and exercise intolerance in these mice. To confirm the critical role of thrombosis in the pathophysiology of diastolic dysfunction, we verified *Lepr<sup>db/db</sup>* also displays increased cardiac microvessel thrombosis. Moreover, consistently, with Dhh deficient mice, we found that aspirin treatment decreased end-diastolic pressure and improved exercise tolerance in *Lepr<sup>db/db</sup>* mice. **Conclusion:** Altogether, these results demonstrate that microvessel thrombosis may participate in the pathophysiology of HFpEF.

## KEYWORDS

Heart Failure, thrombosis, coronary microvasculature, diabetes, Hedgehog

GRAPHIC ABSTRACT



## **NON-STANDARD ABBREVIATIONS AND ACRONYMS**

EF: Ejection fraction  
HFpEF: heart failure with preserved ejection fraction  
HFrEF: heart failure with reduced ejection fraction  
NO: nitric oxide  
EC: endothelial cells  
RT-qPCR: Real-time quantitative polymerase chain reaction  
LDL: Low density lipoproteins  
FITC: Fluorescein Isothiocyanate  
Ct: Cycle threshold  
SMCs: Smooth muscle cells  
EDP: end diastolic pressure  
LVEF: left ventricular ejection fraction  
LV: Left-ventricular  
ESV: end-systolic volume  
EDV: end-diastolic volume  
LVPW: left ventricular posterior wall  
IVS: inter-ventricular septum  
LVID: Left ventricular internal diameter  
WGA: Wheat Germ Agglutinin  
HRP: Horseradish peroxidase  
DAB: diaminobenzidine  
DAPI: (4',6-diamidino-2-phenylindole)  
MEM: Minimum Essential Medium  
DMEM: Dulbecco's Modified Eagle's Medium  
RPMI: Roswell Park Memorial Institute medium  
EBM-2: endothelial basal medium-2  
EGM-2: endothelial growth medium-2  
ATP: Adenosine Triphosphate  
RT-qPCR: Real-time quantitative polymerase chain reaction  
PAGE: Polyacrylamide gel electrophoresis  
KO: knock out  
KD: Knock down

## INTRODUCTION

A significant proportion of patients with clinical syndrome of heart failure (HF) happen to have a normal left ventricular ejection fraction (EF) referred to as heart failure with preserved ejection fraction (HFpEF) as opposed to patients with reduced ejection fraction (HFrEF). HFpEF is characterized by increased arterial and myocardial stiffness and decreased left ventricular (LV) relaxation which causes increased LV end-diastolic pressure with impaired LV filling<sup>1</sup>. In contrast to HFrEF, for which significant advances in understanding etiologies and mechanisms have been made, HFpEF pathophysiology is still poorly understood<sup>2</sup>. HFpEF patients are generally older, more often women, with a high prevalence of cardiovascular and non-cardiovascular comorbidities, such as obesity, metabolic syndrome, type 2 diabetes mellitus, hypertension, atrial fibrillation, or renal dysfunction<sup>3</sup>. At molecular and cellular levels, HFpEF has been associated with cardiac fibrosis, cardiomyocyte hypertrophy and stiffness, microvascular dysfunction, inflammation, decreased bioavailability of nitric oxide (NO), and oxidative stress<sup>4</sup>. In 2013, based on the fact that vascular and microvascular dysfunction is highly prevalent in HFpEF patients, WJ Paulus and C Tschöpe proposed that cardiovascular risk factors would lead to a systemic low-grade inflammation triggering endothelial cells (EC) dysfunction which would in turn, be responsible for cardiac wall stiffening and diastolic dysfunction<sup>5</sup>. Over the last decades, the causal role of EC dysfunction has been supported by preclinical studies in which conditional knock-out (KO) rodents have been used to demonstrate that alterations of EC properties is sufficient to promote diastolic dysfunction. This is the case of Sirtuin 3<sup>6,7</sup> or Sirtuin 1<sup>8</sup> disruption and  $\beta$ 3-Adrenergic Receptor<sup>9</sup> or PDZ Domain Containing Ring Finger 3<sup>10</sup> overexpression in ECs.

However, it is still actually unknown whether EC dysfunction is responsible for diastolic dysfunction in patients or animal models with HFpEF<sup>11</sup>. Notably, WJ Paulus's group proposed that decreased NO synthase 3 (NOS3) activity in ECs would decrease the NO available to activate soluble guanylate cyclase (sGC) in cardiomyocytes leading to decreased cGMP production, protein kinase cGMP-dependent 1 (PRKG1) activity and subsequently Titin phosphorylation, ultimately leading to cardiomyocyte stiffening<sup>5</sup>. However, the negative results of clinical trials aiming at restoring NO/sGC/cGMP signaling in HFpEF patients suggest that this pathway may not have a central role in the pathophysiology of HFpEF<sup>11</sup>. Importantly, endothelial dysfunction does not only design endothelium-dependent vasodilation but any detrimental modification of the endothelial phenotype. Notably, it also designs impaired endothelial barrier properties, endothelial activation, impaired endothelial paracrine activity, or impaired endothelial quiescence.

In the present paper, we used Leptin receptor-deficient female mice ( $Lepr^{db/db}$ ) as a model of HFpEF and performed a transcriptomic analysis of cardiac ECs in order to identify new triggers of cardiac endothelial dysfunction in the setting of type 2 diabetes and obesity. Among genes upregulated in diseased mice, we identified Hedgehog interacting protein-like 1 (Hhip1) which encodes for a decoy receptor for Hedgehog (HH) ligands. Accordingly, we performed a series of experiments to measure the functional consequences of impaired HH signaling in the heart of adult mice.

## METHODS

The authors declare that all supporting data are available within the article and its online supplementary files.

### **Mice**

Lepr<sup>db</sup> mice (BKS.Cg-*Dock7<sup>m</sup>*/+ *Lepr<sup>db</sup>*/+J) were obtained from Charles River laboratories and bred together in our animal facility to obtain Lepr<sup>db/db</sup> and control Lepr<sup>db</sup>/+ mice. Only female were used. Dhh Floxed, Dhh<sup>tm1c(IMPC)lcs</sup>, (Dhh<sup>Flox</sup>) mice were generated at the “Institut Clinique de la Souris” through the International Mouse Phenotyping Consortium (IMPC) from a vector generated by the European conditional mice mutagenesis program, EUCOMM and described before<sup>12</sup>. Smo Floxed, Smo<sup>tm2Amc</sup>/J, (Smo<sup>Flox</sup>), and Tg(Myh6-cre/Esr1\*)1Jmk/J, (Myh6-Cre/ESR1) mice were obtained from the Jackson laboratories.

Tg(Cdh5-cre/ERT2)1Rha, (Cdh5-Cre/ERT2) mice<sup>13</sup> which were a gift from RH. Adams, were maintained under a C57BL/6J background. The Cre recombinase in Cdh5-Cre/ERT2 and Myh6-Cre/ESR1 mice was activated by intraperitoneal injection of 1 mg tamoxifen (Sigma-Aldrich) for 5 consecutive days at 8 weeks of age. Successful and specific activation of the Cre recombinase have been verified before<sup>14</sup>. Except for Lepr<sup>db/db</sup> mice, both male and female were used in equal proportions.

Animal experiments were performed in accordance with the guidelines from Directive 2010/63/EU of the European Parliament on the protection of animals used for scientific purposes and approved by the local Animal Care and Use Committee of Bordeaux University. Mice were either sacrificed by cervical dislocation or exsanguination under deep anesthesia (ketamine 100 mg/kg and xylazine 20 mg/kg, IP). Animal were housed in a conventional facility, on a 12h/12h (light/dark) cycle, with water and food provided ad libitum.

### **Aspirin/clopidogrel therapy**

Mice were randomly assigned to be treated or not with 25 mg/kg/day aspirin (Kardegic®, Sanofi) or Clopidogrel (Arrow Génériques) for 28 days in the drinking water. Treated mice were either 8 week-old Cdh5-Cre/ERT2; Dhh<sup>Flox/Flox</sup> mice or 8 week old Lepr<sup>db/db</sup> mice.

### **Cromolyn Sodium/Cetirizine therapy**

To prevent mast cell degranulation, mice were treated with 50 mg/kg/day cromolyn sodium (Abcam) via intra-peritoneal injections for 28 days. Untreated mice received 0,9% NaCl daily intra-peritoneal injections. To investigate the role of Histamine release by mast cell, mice were treated with 4 mg/kg/day cetirizine (Arrow Génériques) orally (in the drinking water) for 28 days.

### **Treadmill Exercise Exhaustion Test**

Before treadmill experiments, mice were habituated to handling to reduce anxiety. Then, animals were familiarized with running on the treadmill (6-lane treadmill, UGO BASILE S.R.L, Italy) for 3 days: on the first day, mice were trained for 12 minutes running sessions, with gradually increasing speed to a maximum of 18 m/minutes at a 10° inclination. The second and the third days, mice were trained for 18 minutes running sessions with gradually increasing speed to a maximum of 24m/minutes at a 10° inclination. After 3 days of acclimatization to the treadmill exercise, exhaustion and fatigue tests were carried out. After 4 minutes of warm up at a speed of 5m/minutes with a slope fixed at 10° inclination, the speed was increased to 14 m/minutes for 2 minutes. The test consisted of a run at gradually increased speed to a maximum of 32 m/minutes: every 2 minutes the

speed was increased by 2 m/minutes until animals were exhausted. Exhaustion was defined when mice were unable to maintain the pace and spent 10 consecutive seconds in the “fatigue zone.” Therefore, mice were considered exhausted when they remained in the lower part of the treadmill (last third) for 10 seconds. The running time was measured.

### ***Echocardiography***

Left ventricular EF and LV dimension were measured on a high-resolution echocardiographic system equipped with a 30-MHz mechanical transducer (VEVO 2100, VisualSonics Inc) as previously described<sup>15,16</sup>. Mice were anesthetized using 2% oxygenated isoflurane by inhalation. Mice were anchored to a warming platform in a supine position, limbs were taped to the echocardiograph electrodes, and chests were shaved and cleaned with a chemical hair remover to minimize ultrasound attenuation. UNI’GEL ECG (Asept Inmed), from which all air bubbles had been expelled, was applied to the thorax to optimize the visibility of the cardiac chambers. EF was evaluated by planimetry as recommended<sup>17</sup>. Two-dimensional, parasternal long-axis, and short-axis views were acquired, and the endocardial area of each frame was calculated by tracing the endocardial limits in the long-axis view, then the minimal and maximal areas were used to determine the left ventricular end-systolic and end-diastolic volumes, respectively. The system software uses a formula based on a cylindrical- hemi ellipsoid model ( $\text{volume} = 8 \times \text{area}^2 / 3\pi / \text{length}$ ). The left ventricular EF was derived from the following formula:  $(\text{end-diastolic volume} - \text{end-systolic volume}) / \text{end-diastolic volume} \times 100$ . The cardiac wall thickness, LV posterior wall, interventricular septum, and LV internal diameter were calculated by tracing wall limits in both the long and short axis views.

### ***LV Pressure/Systolic Blood Pressure Measurement***

LV diastolic pressure measurement was assessed via invasive catheterization technique. Briefly, mice were anesthetized with 2% isoflurane. A Scisense pressure catheter (Transonic) was inserted into the LV through the common carotid artery. Pressure was recorded using LabChart software. End-diastolic pressure, dP/dt minimum and maximum, Tau, and heart rate were automatically calculated by a curve fit through end-systolic and end-diastolic points on the pressure plot.

### ***Cardiac edema assessment***

After harvest, the heart was dissected to excise the atria, right ventricle and septum. The LV was immediately weighed to measure its wet weight and then incubated for 6 to 8 days at 60°C. At the end, LV dry weight was then measured. LV edema was quantified using the following calculation:  $\text{wet-dry} / \text{wet weight} \times 100$ .

### ***Wire myography***

Femoral arteries, dissected and segmented (1.8-2.0 mm length) were mounted using two tungsten threads in a Mulvany myograph (Danish Myo Technology, Aarhus, Denmark) as previously described<sup>18</sup>. Arteries were bathed in Krebs buffer (119 mmol/L NaCl, 4.7 mmol/L KCl, 1.5 mmol/L CaCl<sub>2</sub>, 1.17 mmol/L MgSO<sub>4</sub>, 1.18 mmol/L KH<sub>2</sub>PO<sub>4</sub>, 25 mmol/L NaHCO<sub>3</sub> and 5.5 mmol/L glucose) and maintained at 37°C. The arteries were studied under a resting tension corresponding to equivalent transmural pressures of 100 mmHg (13.3kPa), which was previously shown to be the optimal resting tension in a passive length-tension relationship. The arteries functionality was checked by adding 80 mmol/L KCl and no difference was observed between the three groups. The relaxant responses to acetylcholine was determined after pre-contraction with phenylephrine (3.10–7M, which corresponds to

approximately 90% of the maximal contraction) by adding increased concentrations (ranging from  $10^{-9}$  to  $10^{-4}$  mol/L) of the vasodilatation agent and by building the concentration/relaxation curve.

### ***Leucocyte Rolling (Live imaging)***

To minimize pain caused by the surgery, mice were subcutaneously administered 0.1 mg/kg buprenorphine 30 min before surgery. Mice were anesthetized by intraperitoneal injection of ketamine (100 mg/kg) and xylazine (10 mg/kg). To label leukocytes, mice were administered intravenously with 3.6 mg/kg Rhodamine 6G (Sigma). Mesenteric venules were then exposed under a stereomicroscope (AXIO Zoom.V16, Zeiss). Leukocyte rolling was imaged at a 200X magnification and 142 frames/second. Three 10-second movies were recorded per mouse. The number of white blood cells crossing a line perpendicular to the vein during 10 seconds was counted. Importantly, white blood cells that are circulating normally are not visible because they are too fast.

### ***Immunostaining***

Prior to harvest, heart was perfused with 8 g/L KCL containing NaCl 0.9% to stop the heart in diastole. The heart was then fixed with methanol, paraffin-embedded and cut into 7  $\mu$ m thick sections. Capillary density was evaluated in sections stained with anti-CD31 or anti-Podocalyxin (PODXL) antibodies by quantifying the number of CD31+ or PODXL+ elements. Leucocyte infiltration was quantified using anti-CD45 antibodies, respectively. Edema was measured after FGB or IgG staining of heart sections and quantified as the mean FGB or IgG-positive areas. Endothelial activation was identified using anti-ICAM-1. Thrombi were identified using anti-CD41 antibodies and quantified as the number of CD41+ elements. (See Supplemental table 1 for antibody references.)

Cardiomyocyte mean surface area was measured using ImageJ software after membrane staining with Wheat Germ Agglutinin (WGA), Alexa Fluor™ 488 Conjugate (Invitrogen). Fibrosis was assessed either after sirius red staining of heart sections by quantifying the percentage of red stained area. Quantifications were done on images were acquired using an Axiozoom V16 or Axioscope A1 (Zeiss) under 200x magnification. They were conducted on 10 randomly selected images were performed using ImageJ/Fiji v2.0.0-rc-59 software (National Institute of Health, USA) by an investigator blinded to genotype. More precisely, each sample received a unique number. At the end of the experiment, the genotype/treatment for each sample was unveiled to enable data analysis.

For immunohistochemical analyses, primary antibodies were sequentially coupled with biotin-conjugated secondary antibodies and streptavidin-horseradish peroxidase (HRP) complex (Amersham). Staining was then revealed with a DAB substrate kit (Vector Laboratories) and tissue sections were counterstained with hematoxylin (see Supplemental table 2 for secondary antibody references).

For immunofluorescence analyses, primary antibodies were identified with Alexa-Fluor–conjugated secondary polyclonal antibodies (see Supplemental table 2). Nuclei were counterstained with DAPI (4',6-diamidino-2-phenylindole).

For both immunohistochemical and immunofluorescence analyses, negative control experiments to check for antibody specificity were performed using secondary antibodies.

Representative confocal images were taken with a ZEISS LSM 700 scanning confocal microscope (Carl Zeiss, Germany).

### ***Isolation of adult mouse cardiac vascular fraction***

Heart were dissociated using 2 mg/mL type IV collagenase (Gibco™, ThermoFisher) for 1 hour at 37°C and the resulting dissociated cells were filtrated on a 30 µm strainer. ECs cells were labelled with rat anti-mouse CD31 microbeads (Miltenyi Biotec) and enriched via magnetic cells sorting.

### ***In situ hybridization***

Prior to harvest, heart was perfused with 8 g/L containing NaCl 0.9% to stop the heart in diastole, it was then fixed with 10% formaline, paraffin-embedded and cut into 5 µm thick sections.

Dhh and Hhip1 mRNA were labeled using the RNAscope® Probe- Mm-Dhh-C2 and RNAscope® Probe- Mm-Hhip1 (Advanced Cell Diagnostcs) respectively. Probe were identified using RNAscope multiplex fluorescent reagent kit V2 and RNA-Protein Co-Detection Ancillary Kit ((Advanced Cell Diagnostcs)) following the manufacturer's instructions.

### ***Quantitative RT-PCR***

RNA was isolated using Tri Reagent (Molecular Research Center Inc) as instructed by the manufacturer, from heart tissue that had been snap-frozen in liquid nitrogen and homogenized. For quantitative real time-polymerase chain reaction (PCR) analyses, total RNA was reverse transcribed with M-MLV reverse transcriptase (Promega), and amplification was performed on an AriaMx Real Time PCR system (Agilent Technologies) using B-R SYBER Green SuperMix (Quanta Biosciences). Primer sequences are reported in Supplemental table 3.

The relative expression of each mRNA was calculated by the comparative threshold cycle method and normalized to b-actin mRNA expression.

### ***RNA sequencing***

RNA was isolated using Tri Reagent® (Molecular Research Center Inc) as instructed by the manufacturer from the cardiac vascular fraction of  $Lepr^{db/db}$  mice and control  $Lepr^{db/+}$  mice. mRNA library preparation were realized following manufacturer's recommendations (KAPA mRNA HyperPrep Kit from ROCHE). Final samples pooled library prep were sequenced on Nextseq 500 ILLUMINA, corresponding to 2x30Millions of reads per sample after demultiplexing. Quality of raw data has been evaluated with FastQC<sup>19</sup>. Poor quality sequences has been trimmed or removed with Trimmomatic<sup>20</sup> software to retain only good quality paired reads. Star v2.5.3a<sup>21</sup> has been used to align reads on mm10 reference genome using standard options. Quantification of gene and isoform abundances has been done with rsem 1.2.28, prior to normalisation with edgeR bioconductor package<sup>22</sup>. Finally, differential analysis has been conducted with the glm framework likelihood ratio test from edgeR. Multiple hypothesis adjusted p-values were calculated with the Benjamini-Hochberg procedure to control FDR. The FPKM values of all transcripts of which expression was significantly different between both groups in Supplemental table 2.

### ***Western Blot Analysis***

ATP2A2 protein level was evaluated by SDS PAGE using rabbit anti-ATP2A2 antibodies (Badrilla, Cat# A010-80). PLN phosphorylation at Serine 16 and Threonin 17 was evaluated by SDS PAGE using rabbit anti-phospho-PLN Ser16 (Badrilla, Cat# A010-12), rabbit anti-phospho-PLN Thr17 (Badrilla, Cat# A010-13) and mouse anti-total PLN (Badrilla, Cat# A010-14).

Protein loading quantity was controlled using mouse monoclonal anti-α-tubulin antibodies (Sigma, Cat# T5168).

### ***Titin Gel***

Tissues were grinded in 8 mol/L Urea buffer (Urea 8 mol/L, Thiourea 2 mol/L, SDS 3%, DTT 75 mmol/L, Tris-HCl 0.05 mol/L, Bromophenol blue 0.03%) and added with glycerol and protease/phosphatase inhibitors. Proteins were then separated on a 1% agarose and 30% glycerol containing gel under a 15 mA intensity for 4 hours at 4°C. The gel was subsequently stained with Pro-Q® Diamond phosphoprotein gel stain to identify phospho-proteins and Coomassie blue to identify total proteins.

### ***Cell culture***

HeLa ATCC® CCL-2™ cells were cultured in Roswell Park Memorial Institute medium (RPMI) supplemented with 10% fetal bovine serum.

NIH/3T3 cells (ATCC CRL-1658™) were cultured in 4.5 g/L containing glucose Dulbecco's Modified Eagle's Medium (DMEM) supplemented with 10% fetal bovine serum. Cells were serum starved in 0.5% fetal bovine serum for 24 hours before any treatments.

Rat Aortic Smooth Muscle Cells (R-ASM-580, Lonza) were cultured in DMEM/F12 medium supplemented with 20% fetal bovine serum. Cells from passages 3 to 10 were used. Cells were serum starved in 0.5% fetal bovine serum for 24 hours before any treatments.

Human umbilical vein endothelial cells (HUVECs) (C2519A, Lonza) were cultured in endothelial basal medium-2 (EBM-2) supplemented with endothelial growth medium (EGM™)-2 BulletKits™ (Lonza). Cells from passages 3 to 6 were used. Cells were serum starved in 0.5% fetal bovine serum containing EBM-2 for 24 hours before any treatments.

### ***Isolation and culture of mouse cardiac fibroblasts***

Hearts were dissociated using 300 U/mL Collagenase type 2 (Worthington) via aortic catheterization and perfusion for 5 minutes at 37°C in 130 mmol/L NaCl, 5.4 mmol/L KCl, 1.4 mmol/L MgCl<sub>2</sub>, 0.4 mmol/L NaH<sub>2</sub>PO<sub>4</sub>, 5 mmol/L HEPES, 10 mmol/L Glucose, 10 mmol/L Creatine, 20 mmol/L Taurine and 0.75 mol/L CaCl<sub>2</sub>. The resulting dissociated cells were then filtrated on a 400 µm mesh and centrifuged at 500 rpm for 5 minutes to separate cardiomyocytes. The supernatant was collected and centrifuged at 1200 rpm for 5 minutes. Cells were re-suspended, plated on plastic and cultured in 1 g/L glucose containing DMEM. Cells from passages 1 to 3 were used. Cells were serum starved in 0.5% fetal bovine serum for 24 hours before any treatments.

### ***Isolation and culture of mouse adult ventricular cardiomyocytes***

Hearts were dissociated using 300 U/mL Collagenase type 2 (Worthington) via aortic catheterization and perfusion for 5 minutes at 37°C in 130 mmol/L NaCl, 5.4 mmol/L KCl, 1.4 mmol/L MgCl<sub>2</sub>, 0.4 mmol/L NaH<sub>2</sub>PO<sub>4</sub>, 5 mmol/L HEPES, 10 mmol/L Glucose, 10 mmol/L Creatine, 20 mmol/L Taurine and 0.75 mol/L CaCl<sub>2</sub>. The resulting dissociated cells were then filtrated on a 400 µm mesh and centrifuged at 500 rpm for 5 minutes to separate cardiomyocytes. Centrifuged cardiomyocytes then incubated in increasing CaCl<sub>2</sub> concentrations (from 12,5 µmol/L to 900 µmol/L in the presence of 2 mmol/L Adenosine Triphosphate (ATP) (Sigma). Cells were then centrifuged again at 500 rpm for 5 minutes, re-suspended in Minimum Essential Medium (MEM) (Gibco) containing 5% FBS, 1.26 mM CaCl<sub>2</sub>, 10 mmol/L 2,3-Butanedione monoxime (Sigma) and 2 mmol/L ATP and seeded in cell culture

wells coated with 10 µg/mL Laminine (Sigma). After a 2-hour incubation at 37°C, culture medium was replaced by MEM containing 0,2% bovine serum albumin (Sigma), 1.26 mM CaCl<sub>2</sub>, 1X Insulin/Transferin/Selenium (Gibco) and 25 µM blebbistatin (Sigma).

### ***Plasmid Transfection***

pcDNA3-FL-Dhh<sup>23</sup> was described previously. The myc-tagged human Ptch1, Ptch1-1B-myc was kindly given by R. Toftgard<sup>24</sup>. pLEICS-29- Hhip1-GFP<sup>25</sup> was kindly given by Tom R Webb. pRK Smo WT<sup>26</sup> was a gift from Baoling Wang. pIRES-NShh<sup>27</sup> was described previously.

HeLa cells were transfected using JetPRIME™ transfection reagent (Polyplus Transfection), according to the manufacturer's instructions. More precisely, 2x10<sup>6</sup> HeLa cells were seeded in a 58 cm<sup>2</sup> cell culture dish. Transfection was done at day +1 with a total of 5 µg of plasmid DNA and 5 µL JetPRIME. Cells were lysed at day+2 for immunoprecipitation assays.

NIH/3T3 cells were transfected using JetPRIME™ transfection reagent (Polyplus Transfection), according to the manufacturer's instructions. More precisely, 4x10<sup>5</sup> NIH/3T3 cells were seeded in a 3.8 cm<sup>2</sup> cell culture well. Transfection was done at day +1 with a total of 1.5 µg of plasmid DNA and 1.5 µL JetPRIME. Cells were serum starved at day+2, treated with N-SHH at Day +3 and RNA samples harvested at day +4.

### ***Preparation of N-SHH containing culture medium.***

HeLa cells were transfected with pIRES-NShh or an empty vector using JetPRIME™ transfection reagent. The following day, cell culture medium was replaced by 4.5 g/L glucose containing DMEM supplemented with 0.5% fetal bovine serum. The N-SHH-containing and control medium were harvested 24 hours later.

### ***siRNA/transfection***

HUVECs were transfected with human DHH siRNA: rArCrUrCrCrUrUrArArArGgArGrArCrUrUrUrUrArGCC, human CAMSAP2 siRNA: 5'-rGrArArArCrArGrTrTrArGrCrCrArCrArTrA-3' or universal scrambled negative control siRNA duplex (Origen) using JetPRIME™ transfection reagent (Polyplus Transfection), according to the manufacturer's instructions.

### ***Immunoprecipitation/western blot analysis***

Prior to western blot analysis, Ptch1 was immunoprecipitated with anti myc-tag antibodies (Millipore, Cat# 05-724). Expression of Dhh, Shh, Ptch1 and Smo were evaluated by SDS PAGE using mouse anti-Dhh antibodies (Santa Cruz Biotechnology, Inc, Cat# sc-271168), mouse anti-Shh antibodies (Santa Cruz Biotechnology, Inc, Cat#sc-365112), rabbit-anti Hh antibodies (Santa Cruz Biotechnology, Inc, Cat# sc-9024), rabbit anti-Ptch1 antibodies (Abcam, Cat#ab53715).

### ***Cardiomyocyte contractility Assay***

Freshly isolated cardiomyocytes (less than 12 hours) were placed in a perfusion chamber mounted on the stage of an inverted microscope (Eclipse Ti-U, Nikon; France) and continuously perfused with a Tyrode solution (140 mmol/L NaCl, 5 mmol/L KCl, 1 mmol/L CaCl<sub>2</sub>, 1 mmol/L MgCl<sub>2</sub>, 10 mmol/L glucose and 10 mmol/L HEPES, pH 7.4) at room temperature. Cardiomyocytes were field-stimulated

to contract at 2 Hz through platinum electrodes connected to a constant-voltage stimulator (DS2A, Digitimer Ltd) and sarcomere length continuously monitored through a video-detection system (MyoCam, IonOptix). Ten consecutive beats at steady-state were averaged and analyzed using IonWizard software (IonOptix).

### Statistics

Results are reported as mean±SEM. Comparisons between groups were analysed for significance with the nonparametric Mann-Whitney test or the Kruskal-Wallis test followed by Dunn multiple comparison test (for >2 groups) using GraphPad Prism v8.0.2 (GraphPad Inc, San Diego, Calif). The normality and variance were not tested. Differences between groups were considered significant when  $P \leq 0.05$  (\* $P \leq 0.05$ ; \*\* $P \leq 0.01$ ; \*\*\* $P \leq 0.001$ ).

## RESULTS

### ***Dhh-induced signaling is impaired in the heart of $Lepr^{db/db}$ mice***

We used  $Lepr^{db/db}$  female mice as a model of diastolic dysfunction<sup>28</sup> to identify new triggers of cardiac microvessel disease associated with this condition. Practically, we performed a transcriptomic analysis, via RNA sequencing of the cardiac vascular fraction of  $Lepr^{db/db}$  mice and compared it to the one of their control littermate  $Lepr^{db/+}$ . Notably, this analysis, which we published previously<sup>28</sup>, revealed that *Hhip1* which encodes for a decoy receptor for HH ligands is significantly upregulated in the heart of  $Lepr^{db/db}$  mice. Interestingly, we previously demonstrated that HH signaling is critical for endothelium integrity<sup>23</sup>. Moreover, this gene has been previously associated with cardiovascular diseases and atherosclerosis in humans in genome-wide association studies<sup>25,29</sup>. First, we confirmed that *Hhip1* mRNA is upregulated in the heart of  $Lepr^{db/db}$  mice via RT-qPCR (Figure 1A) and hypothesized that *Hhip1* overexpression may inhibit HH signaling in the heart of  $Lepr^{db/db}$  by acting as a decoy receptor for HH ligands. Indeed, we found N-SHH-induced *Gli1* overexpression in NIH/3T3 fibroblasts is significantly reduced when *HHIPL1* is overexpressed (Figure S1A) supporting the role of *HHIPL1* as a decoy receptor for HH ligands.

We then search for cells expressing *Hhip1* in the heart by RNAscope® in situ hybridization. As shown in Figure 1B, *Hhip1* is expressed by multiple vascular cells including ECs, SMCs, and fibroblasts. Notably, we found *Hhip1* is expressed by endothelial cells from both arteries (aorta) and capillaries suggesting its expression is not specific for a certain type of ECs. In order to get some clues regarding the mechanism by which *HHIPL1* may be regulated, we treated cultured ECs, SMCs, and fibroblasts by either 4.5 g/L glucose, 12.5 µg/mL Low-density lipoproteins (LDL) or 250 µmol/L palmitate (Figure 1C-E), 3 compounds known to be increased in the setting of type 2 diabetes. We found that *Hhip1* might be upregulated by hyperglycemia in ECs (Figure 1C). Also, we found glucose-induced *HHIPL1* mRNA in HUVECs depends on oxidative stress since glucose no longer increases *HHIPL1* mRNA levels in the presence of the Superoxide dismutase (SOD) mimetic, MnTBAP (Figure S1B).

In order to identify the “target” of *Hhip1*, we quantified the expression of each HH ligand in the heart of  $Lepr^{db/db}$  mice and their control littermate via RT-qPCR. We found the main HH ligand expressed in the heart of adult mice was Desert Hedgehog (DHH); Indian Hedgehog mRNA was only detected at a low level while Sonic Hedgehog mRNA was not expressed (Figure S1C-E). Importantly, *Ihh* and *Shh* primers were validated using intestine (in which *Ihh* mRNA was detected with a cycle

threshold (Ct)=23) and brain (in which *Shh* mRNA was detected with a Ct=24) tissue lysate respectively. *Dhh* and *Ihh* mRNA expression levels were slightly but not significantly downregulated in *Lepr<sup>db/db</sup>* in comparison to control mice. Consistent with our previous investigations, *Dhh* mRNA was mainly detected in ECs, and like *Hhip1*, it is expressed in both arteries and capillaries (Figure S1F). We then tested whether HHIPL1 can bind DHH. To do so we performed co-immunoprecipitation assays using HeLa cells transfected with both DHH and HHIPL1 encoding plasmids. We found HHIPL1 was co-immunoprecipitated with DHH suggesting HHIPL1 can bind DHH (Figure 1F). Finally, we tested whether HHIPL1 can prevent DHH binding to Patched-1 (PTCH1). We performed co-immunoprecipitation assay again and found that the amount of DHH immunoprecipitated together with PTCH1 was significantly diminished in the presence of HHIPL1, suggesting that HHIPL1 prevented DHH binding with PTCH1 (Figure 1G-H).

Altogether these results suggested that the increased HHIPL1 expression observed in cardiac vascular cells in diabetic mice may impair DHH-induced signaling in the heart.

### ***Impaired Dhh-induced signaling induces diastolic dysfunction***

In order to evaluate the functional consequences of impaired DHH-induced signaling in the hearts of adult mice, we used conditional KO mice for DHH. More specifically, we disrupted DHH expression specifically in ECs in 8-week-old mice using *Cdh5-Cre/ERT2* mice. Indeed, we previously demonstrated that DHH is mainly expressed by ECs in the adult mouse heart (Figure S1G)<sup>23</sup>. One month later, *Dhh* mRNA expression was diminished by more than 80% in the cardiac ECs of *Dhh<sup>ECKO</sup>* while neither *Ihh* nor *Shh* mRNA expression was modulated (Figure S1H-I). As a result, *Dhh* mRNA expression in the whole heart was decreased by more than 50% (Figure S1J).

To test whether impaired DHH signaling in the heart may contribute to heart failure, we measured cardiac function in *Dhh<sup>ECKO</sup>* mice and their control littermates, 1 month after *Dhh* KO was induced, via echocardiography and left ventricular catheterization. *Dhh* deficiency did not affect systolic function, since neither LV ejection fraction nor dP/dt maximum were different in *Dhh<sup>ECKO</sup>* mice as compared to control mice (Figure 2A-B). On the contrary, *Dhh* deficiency induced diastolic dysfunction attested by significantly increased end-diastolic pressure, dP/dt minimum and, Tau (Figure 2C-E). Moreover, *Dhh*-deficient mice display impaired exercise tolerance suggesting heart failure (Figure 2F). This was not associated with cardiac hypertrophy (Figure 2G-H).

Altogether, this set of data demonstrates, for the first time, that impaired DHH signaling in the heart may contribute to diastolic dysfunction and heart failure.

### ***Dhh-induced signaling is necessary to prevent capillary leakage and cardiac inflammation***

To investigate mechanisms underlying the development of diastolic dysfunction in *Dhh<sup>ECKO</sup>* mice, we first assessed the phenotype of the cardiac vasculature of *Dhh* deficient mice. Indeed, we previously demonstrated that DHH is critical for endothelium integrity<sup>23</sup>. *DHH* KO in ECs did not modify capillary density (Figure S2A-B), nor endothelium-dependent vaso-relaxation attested by unchanged acetylcholine-induced vaso-relaxation (Figure S2C). Consistent with our previous investigations, *Dhh<sup>ECKO</sup>* induced abnormal vascular leakage; both fibrinogen and IgG extravasation were significantly increased in the heart of *Dhh<sup>ECKO</sup>* mice compared to control mice (Figure S2D-F). However, this abnormal vascular leakage did not lead to cardiac edema since the LV water content was equivalent in both *Dhh<sup>ECKO</sup>* and control mice (Figure S2G).

*Dhh* ECKO increased leucocyte adhesion and rolling on the endothelium, notably in mesenteric veins (Figure S2H), however, it did not increase expression of adhesion molecules, since Intercellular adhesion molecule 1 (*Icam1*) mRNA and protein levels were not modified in the cardiac ECs from *Dhh*<sup>ECKO</sup> mice compared to the one of control mice while Vascular cell adhesion molecule 1 (*Vcam1*) level was decreased (Figure S2I-K). In line with the increased endothelium adhesiveness, the heart of *Dhh*<sup>ECKO</sup> mice was infiltrated by more CD45+ leucocytes (Figure S3A-B). This was associated with an increased C-C Motif Chemokine ligand 5 (*Ccl5*) mRNA expression in total heart extracts (Figure S3C). Also, *Dhh* ECKO enhanced perivascular fibrosis (Figure S3D-E) but not the overall interstitial fibrosis as attested by equal Sirius red+ surface area (Figure S3F) and similar mRNA expression level of Collagen Type I Alpha 1 Chain and Collagen Type III Alpha 1 Chain in *Dhh*<sup>ECKO</sup> and control mice (Figure S3G-H). The increased perivascular fibrosis was, however, associated with increased *Tgfb1* mRNA levels (Figure S3I).

This set of data confirms DHH is necessary to maintain cardiac capillary integrity.

### ***Dhh*-deficiency induced impaired cardiomyocyte contractility**

We then tested whether the phenotype of cardiomyocytes was altered in *Dhh*-deficient mice. The size of cardiomyocytes was equivalent in *Dhh*<sup>ECKO</sup> and in control mice (Figure 3A-B) which is consistent with heart weight and echocardiographic assessments. Expression of Myosin Heavy Chain 6 (*Myh6*) in the heart was not significantly altered while the one of Myosin Heavy Chain 7 (*Myh7*) was significantly decreased (Figure 3C-D). Connexin-43 (*Cx43*) displayed a similar pattern and expression levels in both groups (Figure 3E-F). ATPase Sarcoplasmic/Endoplasmic Reticulum Ca<sup>2+</sup> Transporting (*ATP2A2*) protein expression level was not different in *Dhh*<sup>ECKO</sup> and in control mice (Figure 4A-B). Phosphorylation of Phospholamban (PLN) on Serine 16 was not modified either while phosphorylation of PLN on threonine 17 was significantly diminished (Figure 4C-E) in *Dhh*<sup>ECKO</sup> mice suggesting impaired cardiomyocyte relaxation. Notably, this is consistent with the increased dP/dt min and Tau measured via left ventricular catheterization. To confirm cardiomyocyte relaxation was impaired in *Dhh*<sup>ECKO</sup> mice, we then performed ex vivo cardiomyocyte contractility tests. In these tests, cardiomyocytes from *Dhh*<sup>ECKO</sup> mice showed a decrease in the amplitude of sarcomere shortening (Figure 4F) and a slower relaxation (Figure 4G) compared to cardiomyocytes from control mice; this is consistent with a slower Ca<sup>2+</sup> reuptake by the sarcoplasmic reticulum.

Finally, we tested whether the properties of Titin (TTN) the giant protein controlling cardiomyocyte stiffness were modified. Notably, the ratio of isoform N2BA/N2B of Ttn was significantly increased in *Dhh*<sup>ECKO</sup> mice (Figure 4H-J) while the overall phosphorylation of TTN measured using Pro-Q diamond stain was not modified (Figure 4K-L).

Altogether these results show that impaired cardiac relaxation attested by the increased dP/dt min and Tau values, is associated with a decreased phosphorylation of PLN on Thr17 and a decreased cardiomyocyte relaxation velocity suggesting an impaired calcium reuptake by the sarcomeric reticulum. The increased ratio N2BA/N2B of Ttn isoforms, which is what is typically seen in human heart failure<sup>30</sup>, is more likely reflecting an adaptation of the heart to the increased EDP. The increased *Myh7* expression is unexpected since the opposite is usually seen in heart failure<sup>31</sup>.

***Impaired cardiac relaxation in *Dhh*<sup>ECKO</sup> mice is due to impaired HH signaling to ECs but not cardiomyocytes.***

In order to test whether impaired cardiomyocyte and cardiac wall relaxation observed in *Dhh*<sup>ECKO</sup> mice was due to impaired DHH signaling to cardiomyocytes directly or to impaired DHH signaling to ECs, we used Smoothed (Smo) conditional KO mice. Smo expression was either disrupted in cardiomyocytes by tamoxifen administrations in Myh6-Cre/ESR1, *Smo*<sup>Flox/Flox</sup> (*Smo*<sup>CMKO</sup>) mice or in ECs by tamoxifen administrations in Cdh5-Cre/ERT2, *Smo*<sup>Flox/Flox</sup> (*Smo*<sup>ECKO</sup>) mice. Assessments were performed one month later; at first, we verified that Smo mRNA expression was effectively downregulated in both of these mice (Figure S4A-B), and then, we assessed cardiac function via echocardiography and LV catheterization. Unexpectedly, the LVEF, heart weight over tibia length ratio and EDP were equivalent in *Smo*<sup>CMKO</sup> mice and control littermates (Figure S4C-E) suggesting that the impaired cardiomyocyte relaxation observed in *Dhh*<sup>ECKO</sup> mice is not due to impaired DHH signaling to cardiomyocytes directly. On the contrary, *Smo*<sup>ECKO</sup> mice fully recapitulated the phenotype of *Dhh*<sup>ECKO</sup> mice, i.e. they showed unchanged LVEF and heart weight over tibia length ratio but significantly increased EDP compared to their control littermates (Figure S4F-H) suggesting that cardiomyocyte relaxation impairment observed in *Dhh*<sup>ECKO</sup> mice is indirectly due to impaired DHH-induced autocrine signaling in ECs.

### ***Dhh*<sup>ECKO</sup> mice display a pro-thrombotic phenotype**

In order to identify the potential mechanisms responsible for the impaired cardiomyocyte relaxation observed in *Dhh*<sup>ECKO</sup> mice; we performed a comparative RNA sequencing analysis of total heart extracts from *Dhh*<sup>ECKO</sup> mice and control mice. This analysis identified 87 genes upregulated in *Dhh*<sup>ECKO</sup> mice vs control and 27 genes that were downregulated (Table S4, Figure S5A). Notably, among these genes upregulated, two (Actin Alpha 1, Skeletal Muscle (*Acta1*) and Titin-Cap (*Tcap*)) were involved in skeletal myofibril assembly confirming that the phenotype of cardiomyocyte is modified in these mice. Most interestingly, a biological process enrichment analysis identified 12 genes involved in blood coagulation (Figure S5B). Those genes, which include Glycoprotein Ib Platelet Subunit Alpha (*Gp1ba*), Glycoprotein IX Platelet (*Gp9*), and Glycoprotein V Platelet (*Gp5*), are actually genes specifically expressed by platelets (Figure S5C). These data suggest that there is an abnormal accumulation of platelets in the heart of *Dhh*<sup>ECKO</sup> mice, so we tested whether the endothelium of *Dhh*<sup>ECKO</sup> mice is pro-thrombotic. Accordingly, we found that both the amount of Von Willebrand Factor (VWF) exposed at the surface of the aortic endothelium (Figure 5A-B) or accumulated in the subendothelium of cardiac capillaries (Figure 5C-D) and the level of circulating D-dimers were significantly increased in *Dhh*<sup>ECKO</sup> mice (Figure 5E). Consistent with the RNA sequencing data, the number of thrombi, identified after CD41 staining of heart sections was significantly increased in the coronary microvasculature of *Dhh*<sup>ECKO</sup> mice in comparison to control mice (Figure 5F-G). Notably, in *Dhh*<sup>ECKO</sup> mice CD41 staining was co-localized with FGB staining but not TER119 staining (Figure S6A) suggesting thrombi formed in *Dhh*<sup>ECKO</sup> mice are rather fibrin-rich than red blood cell-rich thrombi. The same phenotype was observed in *Smo*<sup>ECKO</sup> mice. Indeed, like *Dhh*<sup>ECKO</sup> mice, *Smo*<sup>ECKO</sup> mice showed increased VWF released at the surface of the aortic (Figure S6B-C) and increased thrombi density in the heart (Figure S6D-E). In vitro, we confirmed DHH knock-down in cultured ECs increased soluble over cellular VWF (Figure S7A-B) suggesting DHH knock-down promotes Weibel-Palade bodies exocytosis. Mechanistically, we found DHH knock-down downregulates CAMSAP2 (Figure S7C-D) which in turn could promote VWF release (Figure S7E-F). This is consistent with the critical role of microtubules in regulating Weibel-Palade bodies exocytosis<sup>32</sup>.

Altogether these data demonstrated for the first time that impaired DHH-induced signaling in EC promotes thrombosis possibly by increasing Weibel-Palade bodies' exocytosis and VWF release.

To test whether increased thrombi formation in *Dhh*<sup>ECKO</sup> mice could affect the perfusion of the coronary microcirculation, mice were administered intravenously with FITC-labelled BS1-Lectin. As shown in Figure 5H-I, the percentage of cardiac capillaries perfused with BS-1 lectin over 2 minutes was significantly diminished in *Dhh*<sup>ECKO</sup> mice. Moreover, this impaired capillary perfusion was associated with increased levels of Solute Carrier Family 2 Member 1 (Slc2a1), Hypoxia Inducible Factor 1 Subunit Alpha (HIF1A), and Carbonic Anhydrase 9 (CA9), three markers of cardiac hypoxia (Figure 5J-M).

Altogether, these results demonstrate that *Dhh*<sup>ECKO</sup> mice do have a pro-thrombotic phenotype which induces local tissue hypoxia, especially in the heart.

### ***Hypoxia is responsible for Tcap and Acta1 upregulation in cardiomyocytes***

We then hypothesized that the changes in the cardiomyocyte phenotype observed in *Dhh*<sup>ECKO</sup> mice could be either due to some modifications in the EC secretome, an indirect consequence of local tissue hypoxia, or consecutive to cardiac inflammation. To test this hypothesis, we first treated mouse adult cardiomyocytes with conditioned medium from *Dhh*<sup>KO</sup> or control ECs. Conditioned medium from *Dhh*<sup>KO</sup> ECs rather increased than decreased phosphorylation of PLN (Figure S8A-B). Also, it did not modify the mRNA expression of *Tcap* or *Acta1* (Figure S8C-D), the 2 genes involved in skeletal myofibril assembly and identified in the RNA sequencing analysis. To test the potential role of hypoxia, primary cultured mouse adult cardiomyocytes were treated or not with CoCl<sub>2</sub> for 5 hours. As positive controls, we first verified Vascular Endothelial Growth Factor A (*Vegfa*) and *Slc2a1* mRNA were increased in CoCl<sub>2</sub>-treated cardiomyocytes (Figure S8E-F). CoCl<sub>2</sub> treatment did not diminish PLN phosphorylation; on the contrary, it increased it (Figure S8G-H). However, CoCl<sub>2</sub> increased *Tcap* and *Acta1* mRNA levels (Figure S8I-J) suggesting local tissue hypoxia is responsible for *Tcap* and *Acta1* upregulation in cardiomyocytes in *Dhh*<sup>ECKO</sup> mice. CoCl<sub>2</sub> also increased Period Circadian Regulator 2 (*Per2*) mRNA in mouse cardiomyocytes (Figure S8K). Notably, *Per2* which is also upregulated in the heart of *Dhh*<sup>ECKO</sup> mice (Table S4) is known to regulate *Tcap*<sup>33</sup>. Finally, to assess the possible consequences of cardiac inflammation, we treated cardiomyocytes with IL-6 for 5 hours, as shown in Figure S8L-M, IL-6 significantly decreased phosphorylation of PLN on Threonine 17. Moreover, IL-6 also increased expression of Neurogranin mRNA (*Nrgn*) (Figure S8N). Interestingly, NRGN of which mRNA expression is upregulated in the heart of *Dhh*<sup>ECKO</sup> mice (Table S4) is known to inhibit CamKII<sup>34</sup>.

In conclusion, the increased *Tcap* and *Acta1* mRNA expression observed in the heart of *Dhh*<sup>ECKO</sup> mice is likely to be due to local tissue hypoxia while the decreased phosphorylation of PLN is more likely due to cardiac inflammation and NRGN overexpression.

### ***Diastolic dysfunction in Dhh<sup>ECKO</sup> mice is due to increased capillary thrombosis***

With the aim to test whether the increased thrombi formation in *Dhh*<sup>ECKO</sup> mice is responsible for diastolic dysfunction, *Dhh*<sup>ECKO</sup> mice were treated or not with aspirin at a dose of 25 mg/kg/day for 1 month starting the same day they were administered with tamoxifen. First, we verified aspirin treatment did decrease the density of thrombi in the heart (Figure 6A). Then we tested whether diastolic function was improved when mice were treated with aspirin. We found that aspirin-

treatment significantly reduced EDP in *Dhh*<sup>ECKO</sup> mice (Figure 6B). Tau was also diminished without reaching significance (Figure 6C). These results indicate for the first time that thrombosis, which impairs the perfusion of 10% of the cardiac capillaries, contributes to diastolic dysfunction in *Dhh*<sup>ECKO</sup> mice. Consistent with improved heart function, *Dhh*<sup>ECKO</sup> mice treated with aspirin showed significantly improved exercise tolerance when submitted to the treadmill test (Figure 6D). At tissue level, the improved diastolic function in *Dhh*<sup>ECKO</sup> mice treated with aspirin was associated with diminished leukocyte infiltration (Figure 6E) and decreased perivascular fibrosis (Figure 6F) while the increased vascular leakage was not corrected (Figure 6G).

Finally, in order to make sure the effect of aspirin was actually due to its anti-thrombotic activity, *Dhh*<sup>ECKO</sup> mice were treated or not with clopidogrel, another antiplatelet agent, to reduce thrombi formation (Figure S9A). We found that clopidogrel treatment significantly decreased EDP and Tau in *Dhh*<sup>ECKO</sup> mice (Figure S9B-C) confirming the critical role of thrombosis in the development of diastolic dysfunction in *Dhh*<sup>ECKO</sup> mice.

### ***Antiplatelet therapies prevent the occurrence of diastolic dysfunction in *Lepr*<sup>db/db</sup> mice***

Finally, in order to test whether the results we obtained in *Dhh*<sup>ECKO</sup> mice were also relevant in *Lepr*<sup>db/db</sup> mice; we first quantified thrombi in the heart and *Lepr*<sup>db/db</sup> female mice and in their control littermate. We found that thrombi density was significantly increased in the heart of *Lepr*<sup>db/db</sup> mice in comparison to control mice (Figure 7A-B) and associated with increased HIF1A levels (Figure 7C-D). Then, we used two antiplatelet therapies to test whether thrombi formation participated in the pathophysiology of diastolic dysfunction in these mice. *Lepr*<sup>db/db</sup> mice were either treated with aspirin (25 mg/kg/day) or clopidogrel (5 mg/kg/day) for 28 days starting at 8 weeks of age. We found that *Lepr*<sup>db/db</sup> mice treated with either aspirin or clopidogrel showed significantly decreased EDP in comparison to vehicle-treated mice (Figure 7E). Consistently, aspirin and clopidogrel-treated *Lepr*<sup>db/db</sup> mice also showed improved Tau (Figure 7F) and significantly increased exercise tolerance (Figure 7G).

This set of data demonstrates for the first time that thrombosis may contribute to the development of diastolic dysfunction at least in the setting of type 2 diabetes.

### ***Increased thrombi formation is upstream of mast cell activation in *Lepr*<sup>db/db</sup> mice***

We previously demonstrated diastolic dysfunction is triggered by mast cell activation in *Lepr*<sup>db/db</sup> female mice<sup>28</sup>. We then tested whether microvessels thrombosis is upstream, downstream, or independent of thrombi formation in *Lepr*<sup>db/db</sup> mice. To do so, we quantified mast cell degranulation in *Lepr*<sup>db/db</sup> mice treated or not with aspirin and clopidogrel and thrombi density in cromolyn sodium and cetirizine-treated mice. We found aspirin or clopidogrel treatment prevented mast cell activation (Figure S10A) while cromolyn sodium or cetirizine treatment did not modify thrombi density (Figure S10B) in *Lepr*<sup>db/db</sup> mice suggesting mast cell activation occurs subsequently to thrombi formation in these mice.

## **DISCUSSION**

The present study highlights for the first time the critical role of microvessel thrombosis in the pathophysiology of diastolic dysfunction and identifies an original mechanism involving a HH signaling impairment in ECs. Notably, endothelial dysfunction was proposed to be responsible for HFpEF about 10 years ago in the paradigm proposed by Paulus et al in 2013<sup>5</sup>, however, the pro-

thrombotic phenotype of ECs has never been considered as a pathophysiological mechanism responsible for diastolic dysfunction.

Mechanistically, our study reveals that *Hhip1*, a gene previously associated with cardiovascular diseases<sup>35</sup> and cardiometabolic risk parameters<sup>36</sup> in genome-wide association studies in humans is upregulated in *Lepr<sup>db/db</sup>* diabetic obese mice. HHPL1 overexpression negatively regulates DHH-induced signaling in ECs, which causes VWF release and promotes thrombosis notably in the coronary microvasculature. The subsequent impaired capillary perfusion induces cardiac hypoxia and inflammation which affects cardiomyocyte biology and impairs cardiac relaxation. Indeed, in *Dhh<sup>ECKO</sup>* mice, cardiomyocytes display decreased phosphorylation of PLN on Thr17 and impaired cardiomyocyte contractility. Importantly, we used SMO conditional KO mice and performed *in vitro* experiments to demonstrate that diastolic dysfunction occurs because of impaired HH signaling in ECs and that cardiac hypoxia and inflammation are likely responsible for impaired cardiomyocyte relaxation.

Interestingly, even though microvessel thrombosis has never been involved in the pathophysiology of HFpEF before, several recent clinical studies have revealed either that platelet indices notably the mean platelet volume and the platelet to leucocyte ratio<sup>37</sup> or VWF levels<sup>38 39</sup> are strongly associated with worse patient outcome in HFpEF. Consistently, circulating P-selectin level has been shown to be a predictor of mortality in HFpEF<sup>40</sup>. This data fully supports the relevance of our data.

We previously demonstrated that HH signaling, especially DHH-induced signaling in ECs, is critical for endothelium integrity in adult mice<sup>12</sup>. The present study confirms this result and further characterizes DHH effects in ECs. Indeed, we confirmed endothelial-derived DHH is necessary for intercellular junction integrity<sup>23,41</sup>, moreover, we found DHH has antithrombotic properties. Mechanistically, DHH might prevent Weibel-Palade body exocytosis by regulating the stability of microtubules through the regulation of CAMSAP2. Consistently, KLF2 which we previously demonstrated to be upstream of DHH<sup>23</sup> was also shown to regulate Weibel-Palade body exocytosis and VWF release in ECs<sup>42</sup>. Besides CAMSAP2 is a protein regulating microtubule stability which has recently been shown to regulate endothelial cell properties<sup>43</sup>.

However, we did not confirm DHH decreases the expression of adhesion molecules in ECs<sup>12</sup>. On the contrary, we found that DHH, knockdown significantly decreased *Vcam1* and Selectin E (*Sele*) levels (data not shown) while it does not modulate *Icam1* mRNA level; However, consistent with our previous investigation, we found that *Dhh<sup>ECKO</sup>* mice have a pro-adhesive endothelium and display increased leucocyte infiltration in the heart. The increased adhesive properties of *Dhh* KO ECs may then be due to the increased VWF release which has previously been reported<sup>44</sup>. Alternatively, activated platelets may promote monocyte adhesion on the endothelium by releasing CCL5<sup>45</sup> which is consistent with the increased levels of CCL5 we observed in the heart of *Dhh<sup>ECKO</sup>* mice.

Considering the critical role of DHH in maintaining endothelial integrity, impaired HH signaling in adults may participate in the pathophysiology of multiple cardiovascular and cerebrovascular diseases. Notably, we and others previously demonstrated impaired DHH-induced signaling may participate in the pathophysiology of diabetic neuropathy<sup>46,47</sup>. Also, we found that the deregulation of HH signaling at the blood-brain barrier participates in the pathophysiology of multiple sclerosis<sup>41,48</sup>. The present study identifies the critical role of DHH-induced signaling in the adult heart. Regulation of DHH binding with its receptor Patched-1 (PTCH1) is controlled by multiple co-receptors<sup>14</sup> but also by the other HH ligands including Sonic Hedgehog (SHH)<sup>41</sup>. SHH has often been shown to

be upregulated in several acute stress conditions<sup>41,49</sup>, however, the mechanism by which it occurs is unknown. We previously demonstrated Cell-Adhesion Associated, Oncogene-Regulated (CDON), a decoy receptor for DHH is upregulated by inflammatory cytokines<sup>14</sup>. HHIPL1, another decoy receptor for DHH was shown to be upregulated in atherosclerotic plaques<sup>25</sup>. In the present study, we found that it is also upregulated in *Lepr<sup>db/db</sup>* mice, in several vascular cells including endothelial cells in which it might be upregulated by hyperglycemia. In summary, the mechanisms leading to impaired DHH-induced signaling in ECs are multiple and still poorly understood, therefore, DHH-induced signaling impairment is still difficult to predict but should be considered as an important actor of cardiovascular and cerebrovascular diseases. Besides, the mechanism of action of HHIPL1 is still unclear since our data suggest it may act as a decoy receptor while in the study conducted by Aravani D. and collaborators, it was proposed to promote HH signaling. One explanation for this is that, while Aravani D and collaborators measured the effect of soluble HHIPL1 only, we evaluated the effect of both soluble and membrane-bound HHIPL1.

In conclusion, the present study characterizes an original mechanism contributing to the pathophysiology of diastolic dysfunction in *Lepr<sup>db/db</sup>* mice and identifies thrombosis as a new therapeutic target for HFpEF patient care.

#### **ACKNOWLEDGMENTS**

We thank Annabel Reynaud, Sylvain Grolleau, and Maxime David for their technical help. This work benefited from equipment and services from the iGenSeq (RNA sequencing) and iCONICS (RNAseq analysis) core facilities at the ICM (Institut du Cerveau et de la Moelle épinière, Hôpital Pitié-Salpêtrière, PARIS, France).

#### **SOURCES OF FUNDING**

This study was supported by grants from the Fondation pour la Recherche Médicale (équipe FRM), the Agence Nationale pour la Recherche (Appel à Projet Générique) and the Région Nouvelle Aquitaine. Additionally, this study was co-funded by the “*Institut National de la Santé et de la Recherche Médicale*” (Inserm), and by the University of Bordeaux.

#### **DISCLOSURES**

none

#### **SUPPLEMENTAL MATERIAL**

Detailed Methods

Figure S1-S10

Tables S1–S4

Major Resources Table

#### **REFERENCES**

1. Zhou Y, Zhu Y, Zeng J. Research Update on the Pathophysiological Mechanisms of Heart Failure with Preserved Ejection Fraction. *Curr Mol Med*. 2023;23:54–62.
2. Lyle MA, Brozovich FV. HFpEF, a Disease of the Vasculature: A Closer Look at the Other Half. *Mayo Clin Proc*. 2018;93:1305–1314.
3. Groenewegen A, Rutten FH, Mosterd A, Hoes AW. Epidemiology of heart failure. *Eur J Heart Fail*. 2020;22:1342–1356.
4. Zhou Y, Zhu Y, Zeng J. Research Update on the Pathophysiological Mechanisms of Heart Failure with Preserved Ejection Fraction. *Curr Mol Med*. 2021.  
doi:10.2174/1566524021666211129111202.
5. Paulus WJ, Tschope C. A novel paradigm for heart failure with preserved ejection fraction: comorbidities drive myocardial dysfunction and remodeling through coronary microvascular endothelial inflammation. *J Am Coll Cardiol*. 2013;62:263–71.
6. He X, Zeng H, Chen ST, Roman RJ, Aschner JL, Didion S, Chen J-X. Endothelial Specific SIRT3 Deletion Impairs Glycolysis and Angiogenesis and Causes Diastolic Dysfunction. *J Mol Cell Cardiol*. 2017;112:104–113.
7. Zeng H, He X, Chen J-X. A Sex-Specific Role of Endothelial Sirtuin 3 on Blood Pressure and Diastolic Dysfunction in Female Mice. *Int J Mol Sci*. 2020;21:9744.
8. Maizel J, Xavier S, Chen J, Lin CHS, Vasko R, Goligorsky MS. Sirtuin 1 ablation in endothelial cells is associated with impaired angiogenesis and diastolic dysfunction. *Am J Physiol Heart Circ Physiol*. 2014;307:H1691–H1704.
9. Dhot J, Ferron M, Prat V, Persello A, Roul D, Stévant D, Guijarro D, Piriou N, Aillerie V, Erraud A et al. Overexpression of endothelial  $\beta_3$ -adrenergic receptor induces diastolic dysfunction in rats. *ESC Heart Fail*. 2020;7:4159–4171.
10. Abelanet A, Camoin M, Rubin S, Bougaran P, Delobel V, Pernot M, Forfar I, Guilbeau-Frugier C, Galès C, Bats ML et al. Increased Capillary Permeability in Heart Induces Diastolic Dysfunction Independently of Inflammation, Fibrosis, or Cardiomyocyte Dysfunction. *Arterioscler Thromb Vasc Biol*. 2022;:101161ATVBAHA121317319.
11. Cornuault L, Rouault P, Dupl a C, Couffinhal T, Renault M-A. Endothelial Dysfunction in Heart Failure With Preserved Ejection Fraction: What are the Experimental Proofs? *Frontiers in Physiology*. 2022;13. Available at <https://www.frontiersin.org/articles/10.3389/fphys.2022.906272>. Accessed July 8, 2022.
12. Caradu C, Couffinhal T, Chapouly C, Guimbal S, Hollier P-L, Ducasse E, Bura-Rivi re A, Dubois M, Gadeau A-P, Renault M-A. Restoring Endothelial Function by Targeting Desert Hedgehog Downstream of Klf2 Improves Critical Limb Ischemia in Adults. *Circ Res*. 2018;123:1053–1065.
13. Azzoni E, Conti V, Campana L, Dellavalle A, Adams RH, Cossu G, Brunelli S. Hemogenic endothelium generates mesoangioblasts that contribute to several mesodermal lineages in vivo. *Development*. 2014;141:1821–34.
14. Chapouly C, Hollier P-L, Guimbal S, Cornuault L, Gadeau A-P, Renault M-A. Desert Hedgehog-Driven Endothelium Integrity Is Enhanced by Gas1 (Growth Arrest-Specific 1) but Negatively

Regulated by Cdon (Cell Adhesion Molecule-Related/Downregulated by Oncogenes). *Arterioscler Thromb Vasc Biol.* 2020;40:e336–e349.

15. Renault MA, Roncalli J, Tongers J, Misener S, Thorne T, Jujo K, Ito A, Clarke T, Fung C, Millay M et al. The Hedgehog transcription factor Gli3 modulates angiogenesis. *Circ Res.* 2009;105:818–26.
16. Roncalli J, Renault MA, Tongers J, Misener S, Thorne T, Kamide C, Jujo K, Tanaka T, Li M, Klyachko E et al. Sonic hedgehog-induced functional recovery after myocardial infarction is enhanced by AMD3100-mediated progenitor-cell mobilization. *J Am Coll Cardiol.* 2011;57:2444–52.
17. Schiller NB, Shah PM, Crawford M, DeMaria A, Devereux R, Feigenbaum H, Gutgesell H, Reichek N, Sahn D, Schnittger I. Recommendations for quantitation of the left ventricle by two-dimensional echocardiography. American Society of Echocardiography Committee on Standards, Subcommittee on Quantitation of Two-Dimensional Echocardiograms. *J Am Soc Echocardiogr.* 1989;2:358–367.
18. Dumas de la Roque E, Smeralda G, Quignard J-F, Freund-Michel V, Courtois A, Marthan R, Muller B, Guibert C, Dubois M. Altered vasoreactivity in neonatal rats with pulmonary hypertension associated with bronchopulmonary dysplasia: Implication of both eNOS phosphorylation and calcium signaling. *PLoS One.* 2017;12:e0173044.
19. Andrews S. FastQC: a quality control tool for high throughput sequence data. .
20. Bolger AM, Lohse M, Usadel B. Trimmomatic: a flexible trimmer for Illumina sequence data. *Bioinformatics.* 2014;30:2114–2120.
21. Dobin A, Davis CA, Schlesinger F, Drenkow J, Zaleski C, Jha S, Batut P, Chaisson M, Gingeras TR. STAR: ultrafast universal RNA-seq aligner. *Bioinformatics.* 2013;29:15–21.
22. Robinson MD, McCarthy DJ, Smyth GK. edgeR: a Bioconductor package for differential expression analysis of digital gene expression data. *Bioinformatics.* 2010;26:139–140.
23. Caradu C, Couffignal T, Chapouly C, Guimbal S, Hollier P-L, Ducasse E, Bura-Rivière A, Dubois M, Gadeau A-P, Renault M-A. Restoring Endothelial Function by Targeting Desert Hedgehog Downstream of Klf2 Improves Critical Limb Ischemia in Adults. *Circ Res.* 2018;123:1053–1065.
24. Kogerman P, Krause D, Rahnema F, Kogerman L, Undén AB, Zaphiropoulos PG, Toftgård R. Alternative first exons of PTCH1 are differentially regulated in vivo and may confer different functions to the PTCH1 protein. *Oncogene.* 2002;21:6007–6016.
25. Aravani D, Morris GE, Jones PD, Tattersall HK, Karamanavi E, Kaiser MA, Kostogrysb RB, Ghaderi Najafabadi M, Andrews SL, Nath M, Ye S, Stringer EJ, Samani NJ, Webb TR. HHIPL1, a Gene at the 14q32 Coronary Artery Disease Locus, Positively Regulates Hedgehog Signaling and Promotes Atherosclerosis. *Circulation.* 2019;140:500–513.
26. Low WC, Wang C, Pan Y, Huang XY, Chen JK, Wang B. The decoupling of Smoothed from Galphai proteins has little effect on Gli3 protein processing and Hedgehog-regulated chick neural tube patterning. *Developmental biology.* 2008;321:188–96.
27. Caradu C, Guy A, James C, Reynaud A, Gadeau AP, Renault MA. Endogenous Sonic Hedgehog limits inflammation and angiogenesis in the ischemic skeletal muscle of mice. *Cardiovascular research.* 2018;114. doi:10.1093/cvr/cvy017 4819254 [pii].

28. Guimbal S, Cornuault L, Rouault P, Hollier P-L, Chapouly C, Bats M-L, Imbault J, Gadeau A-P, Couffinhal T, Renault M-A. Mast Cells Are the Trigger of Small Vessel Disease and Diastolic Dysfunction in Diabetic Obese Mice. *Arterioscler Thromb Vasc Biol.* 2021;41:e193–e207.
29. Schunkert H, König IR, Kathiresan S, Reilly MP, Assimes TL, Holm H, Preuss M, Stewart AFR, Barbalic M, Gieger C et al. Large-scale association analysis identifies 13 new susceptibility loci for coronary artery disease. *Nat Genet.* 2011;43:333–338.
30. Makarenko I, Opitz CA, Leake MC, Neagoie C, Kulke M, Gwathmey JK, del Monte F, Hajjar RJ, Linke WA. Passive stiffness changes caused by upregulation of compliant titin isoforms in human dilated cardiomyopathy hearts. *Circ Res.* 2004;95:708–716.
31. Vigil-Garcia M, Demkes CJ, Eding JEC, Versteeg D, de Ruiter H, Perini I, Kooijman L, Gladka MM, Asselbergs FW, Vink A et al. Gene expression profiling of hypertrophic cardiomyocytes identifies new players in pathological remodelling. *Cardiovasc Res.* 2021;117:1532–1545.
32. Lovelace MD, Powter EE, Coleman PR, Zhao Y, Parker A, Chang GH, Lay AJ, Hunter J, McGrath AP, Jormakka M et al. The RhoGAP protein ARHGAP18/SENEX localizes to microtubules and regulates their stability in endothelial cells. *Mol Biol Cell.* 2017;28:1066–1078.
33. Podobed PS, Alibhai FJ, Chow C-W, Martino TA. Circadian regulation of myocardial sarcomeric Titin-cap (Tcap, telethonin): identification of cardiac clock-controlled genes using open access bioinformatics data. *PLoS One.* 2014;9:e104907.
34. Jorgensen AN, Abdullah CS, Bhuiyan MS, Watt M, Dominic P, Kolluru GK, Kevil CG, Nam HW. Neurogranin regulates calcium-dependent cardiac hypertrophy. *Exp Mol Pathol.* 2022;127:104815.
35. Schunkert H, König IR, Kathiresan S, Reilly MP, Assimes TL, Holm H, Preuss M, Stewart AFR, Barbalic M, Gieger C et al. Large-scale association analyses identifies 13 new susceptibility loci for coronary artery disease. *Nature genetics.*;43:333.
36. Rodríguez-Pérez JM, Posadas-Sánchez R, Blachman-Braun R, Vargas-Alarcón G, Posadas-Romero C, Rodríguez-Cortés AA, López-Bautista F, Tovilla-Zárate CA, Rojas-Toledo EX, Borgonio-Cuadra VM et al. HHIPL-1 (rs2895811) gene polymorphism is associated with cardiovascular risk factors and cardiometabolic parameters in Mexicans patients with myocardial infarction. *Gene.* 2018;663:34–40.
37. Dahlen B, Schulz A, Göbel S, Tröbs S-O, Schwuchow-Thonke S, Spronk HM, Prochaska JH, Arnold N, Lackner KJ, Gori T et al. The impact of platelet indices on clinical outcome in heart failure: results from the MyoVasc study. *ESC Heart Fail.* 2021;8:2991–3001.
38. Abudoukelimu M, Ba B, Kai Guo Y, Xu J. Von Willebrand factor (vWF) in patients with heart failure with preserved ejection fraction (HFpEF): A retrospective observational study. *Medicine (Baltimore).* 2022;101:e29854.
39. Kleber ME, Koller L, Goliash G, Sulzgruber P, Scharnagl H, Silbernagel G, Grammer TB, Delgado G, Tomaschitz A, Pilz S et al. Von Willebrand factor improves risk prediction in addition to N-terminal pro-B-type natriuretic peptide in patients referred to coronary angiography and signs and symptoms of heart failure and preserved ejection fraction. *Circ Heart Fail.* 2015;8:25–32.

40. Kanagala P, Arnold JR, Khan JN, Singh A, Gulsin GS, Squire IB, McCann GP, Ng LL. Plasma P-selectin is a predictor of mortality in heart failure with preserved ejection fraction. *ESC Heart Fail.* 2021;8:2328–2333.
41. Hollier P-L, Chapouly C, Diop A, Guimbal S, Cornuault L, Gadeau A-P, Renault M-A. Full-length Dhh and N-terminal Shh act as competitive antagonists to regulate angiogenesis and vascular permeability. *Cardiovasc Res.* 2021;117:2489–2501.
42. Ferraro F, Mafalda Lopes da S, Grimes W, Lee HK, Ketteler R, Kriston-Vizi J, Cutler DF. Weibel-Palade body size modulates the adhesive activity of its von Willebrand Factor cargo in cultured endothelial cells. *Sci Rep.* 2016;6:32473.
43. Martin M, Veloso A, Wu J, Katrukha EA, Akhmanova A. Control of endothelial cell polarity and sprouting angiogenesis by non-centrosomal microtubules. *Elife.* 2018;7:e33864.
44. Chauhan AK, Kisucka J, Brill A, Walsh MT, Scheiflinger F, Wagner DD. ADAMTS13: a new link between thrombosis and inflammation. *J Exp Med.* 2008;205:2065–2074.
45. von Hundelshausen P, Weber KS, Huo Y, Proudfoot AE, Nelson PJ, Ley K, Weber C. RANTES deposition by platelets triggers monocyte arrest on inflamed and atherosclerotic endothelium. *Circulation.* 2001;103:1772–1777.
46. Chapouly C, Yao Q, Vandierdonck S, Larrieu-Lahargue F, Mariani JN, Gadeau AP, Renault MA. Impaired Hedgehog signalling-induced endothelial dysfunction is sufficient to induce neuropathy: implication in diabetes. *Cardiovascular research.* 2016;109:217–27.
47. Calcutt NA, Allendoerfer KL, Mizisin AP, Middlemas A, Freshwater JD, Burgers M, Ranciato R, Delcroix JD, Taylor FR, Shapiro R et al. Therapeutic efficacy of sonic hedgehog protein in experimental diabetic neuropathy. *J Clin Invest.* 2003;111:507–14.
48. Mora P, Hollier P-L, Guimbal S, Abelanet A, Diop A, Cornuault L, Couffignal T, Horng S, Gadeau A-P, Renault M-A et al. Blood–brain barrier genetic disruption leads to protective barrier formation at the Glia Limitans. *PLoS Biol.* 2020;18:e3000946.
49. Renault MA, Chapouly C, Yao Q, Larrieu-Lahargue F, Vandierdonck S, Reynaud A, Petit M, Jaspard-Vinassa B, Belloc I, Traiffort E et al. Desert hedgehog promotes ischemia-induced angiogenesis by ensuring peripheral nerve survival. *Circ Res.* 2013;112:762–70.

## HIGHLIGHTS

- Endothelial cells may cause diastolic dysfunction when they acquire a pro-thrombotic phenotype which impairs perfusion of the coronary microvasculature.
- Thrombosis in the coronary microvasculature may induce diastolic dysfunction at least in the setting of type 2 diabetes.
- Thrombosis occurs upstream of mast cell activation in the cascade of event leading to diastolic dysfunction in  $Lepr^{db/db}$  mice.
- DHH prevents endothelial cells from acquiring a pro-thrombotic phenotype by regulating Weibel-Palade body exocytosis.
- Impaired cardiomyocyte relaxation may be induced subsequent to cardiac inflammation and hypoxia. Cardiac inflammation inhibits phosphorylation of PLN, while cardiac hypoxia enhances ACTA1 and TCAP expression.

**FIGURE LEGENDS**

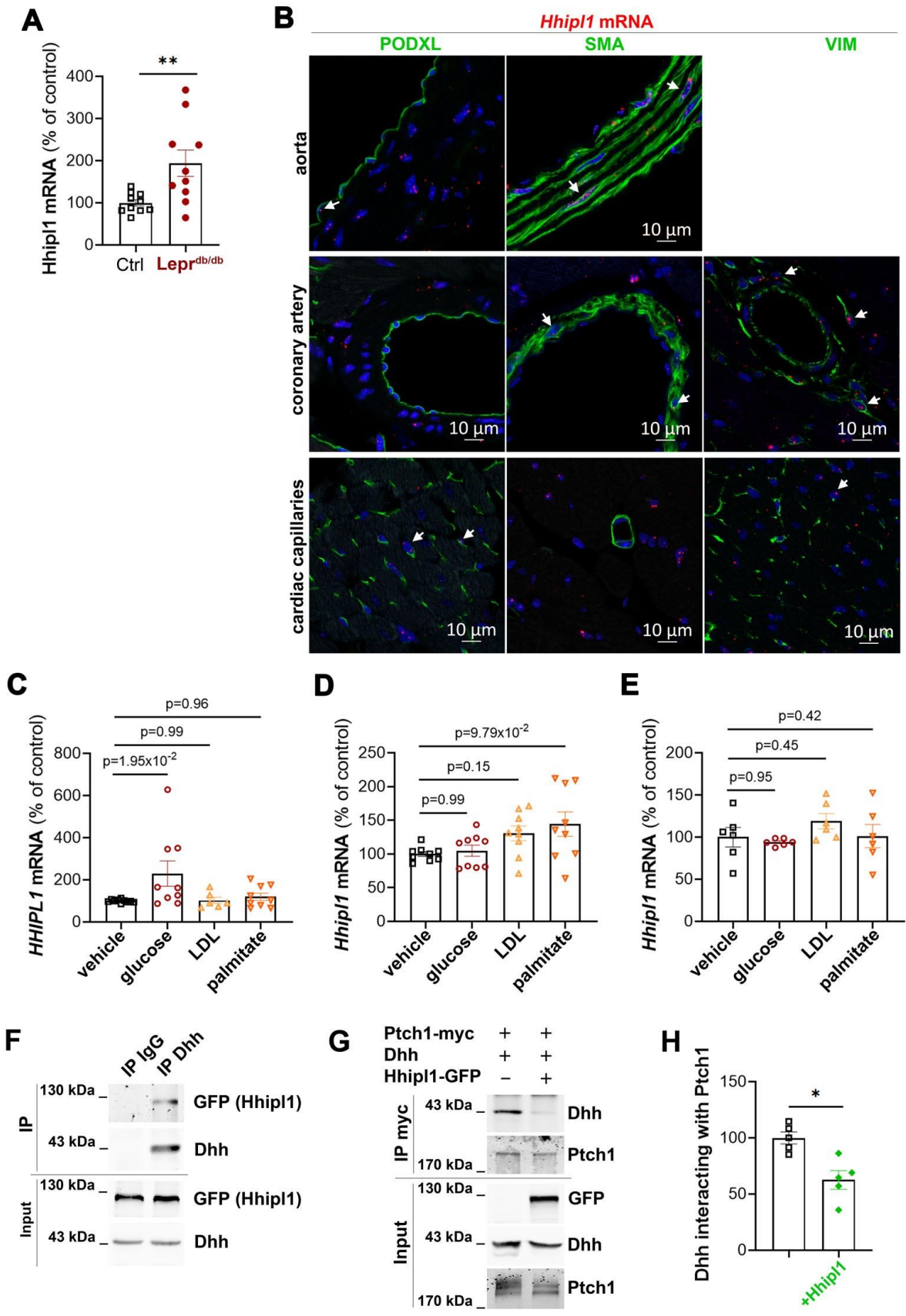


**Figure 1: *Lepr*<sup>db/db</sup> mice display impaired HH signaling in the heart.** (A) *Lepr*<sup>db/db</sup> female mice and their control (*Lepr*<sup>db/+</sup>) littermate were sacrificed at 3 months of age. *Hhip1* mRNA expression was quantified by RT-qPCR in total heart extract and normalized to *Actb* mRNA (n=10 mice per group). (B) Heart sections from 12 week-old *Lepr*<sup>db/db</sup> mice were incubated with *Hhip1* RNA probes (stained in red) together with anti-PODXL antibodies to identify ECs, anti-SMA antibodies to identify SMCs or anti-VIM antibodies to identify fibroblasts (stained in green). Sections were counterstained with DAPI in blue. (C) HUVECs, (D) rat aortic SMCs or (E) cardiac fibroblasts were treated or not with 4.5 g/L glucose, 12,5 µg/L LDL, 250 mmol/L palmitate for 24 hours. *Hhip1* mRNA expression were quantified by RT-qPCR and normalized to *Actb* mRNA (n=6-9 cell culture well per conditions). (F) HeLa cells were co-transfected with *Hhip1*-GFP and FL-Dhh encoding plasmids. Dhh interaction with *Hhip1* was assessed by co-immunoprecipitation assay. (G-H) HeLa cells were co-transfected *Ptch1*-myc and FL-Dhh encoding plasmids together with or without *Hhip1*-GFP encoding plasmids. (G) DHH interaction with PTCH1 was assessed by co-immunoprecipitation assay and (H) quantified using Image J software. The experiment was repeated 5 times. Mann-Whitney test.

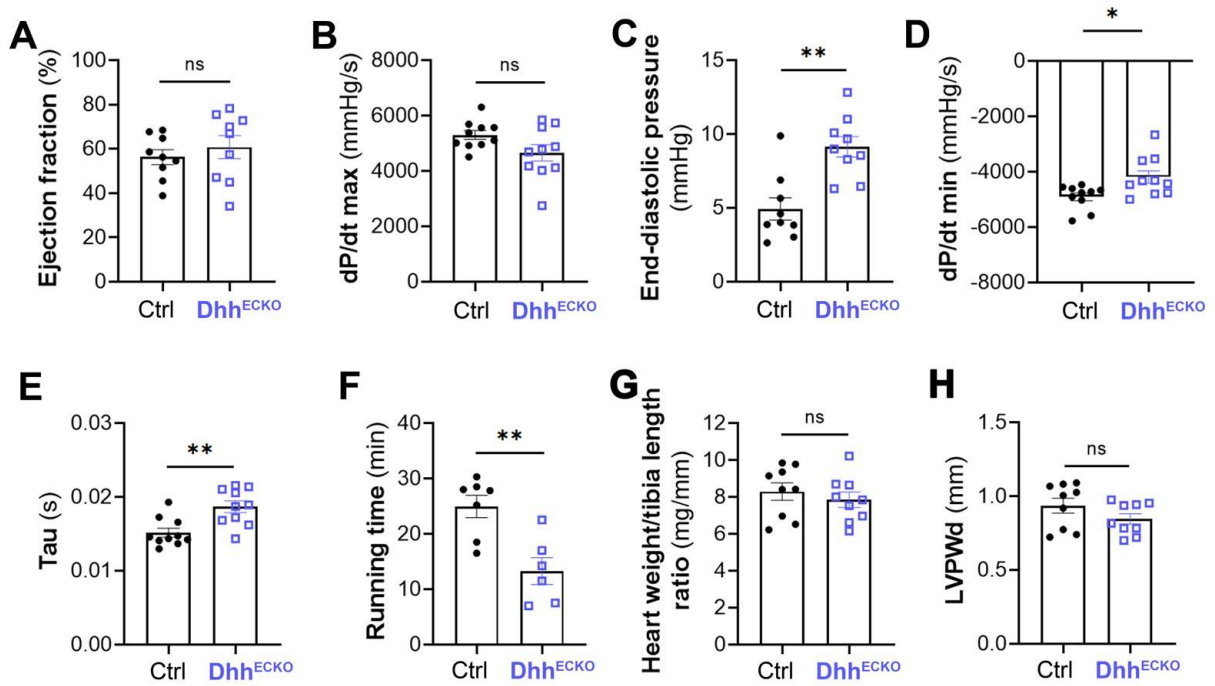


**Figure 2: *Dhh*<sup>ECKO</sup> mice develop diastolic dysfunction.** *Cdh5-Cre/ERT2; Dhh*<sup>Flox/Flox</sup> (*Dhh*<sup>ECKO</sup>) mice and their control littermate (*Dhh*<sup>Flox/Flox</sup>) were administered with tamoxifen at 8 weeks of age. Their cardiac function was assessed one month later. (A) Ejection fraction was assessed via echocardiography (n= 10 mice per group). (B) dP/dt maximum was measured by left ventricular catheterization (n= 10 mice per group) (C) LV end diastolic pressure (EDP) was measured by left ventricular catheterization (n=10 mice per group). (D) dP/dt minimum was measured by left ventricular catheterization (n= 10 mice per group). (E) Tau was measured by left ventricular catheterization (n=10 mice per group). (F) Running time was assessed on treadmill (n=6 and 7 mice per group). (G) The heart weight over tibia length ratio was calculated (n=10 mice per group). (H) Diastolic left ventricular posterior wall (LVPWd) thickness was measured by echocardiography (n=10 mice per group). Mann-Whitney test.

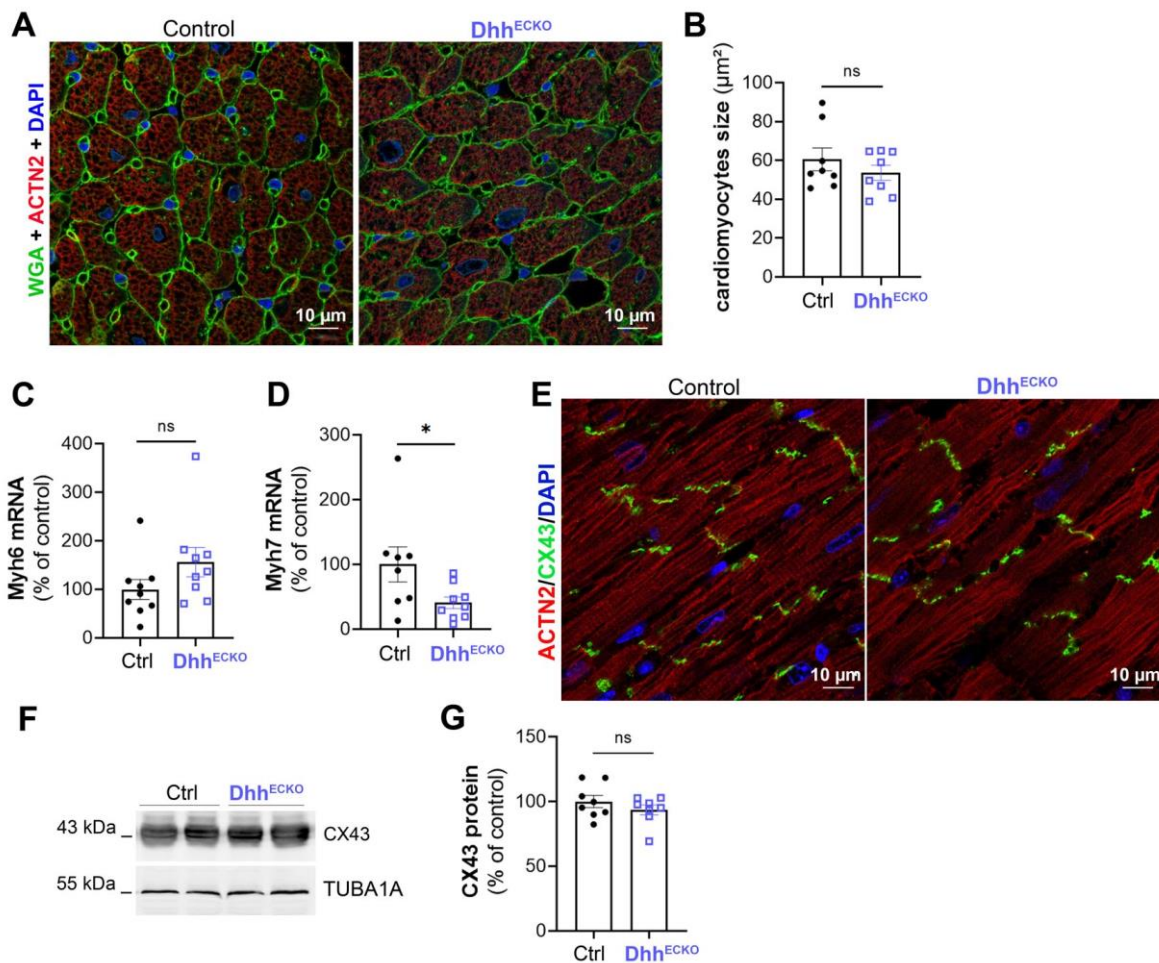


**Figure 3: *Dhh*<sup>ECKO</sup> mice do not display cardiomyocyte hypertrophy.** *Cdh5-Cre/ERT2; Dhh*<sup>Flox/Flox</sup> (*Dhh*<sup>ECKO</sup>) mice and their control littermate (*Dhh*<sup>Flox/Flox</sup>) were administered with tamoxifen at 8 weeks of age and sacrificed at 12 weeks of age. (A) Heart cross sections were co-stained with FITC-labelled WGA and anti-Actinin Alpha 2 (ACTN2) antibodies. (B) Cardiomyocyte cross section area was measured using Image J software (n=8 mouse per group). (C) Myh6 and (D) Myh7 mRNA expression were quantified by RT-qPCR in total heart extract and normalized to *Actb* mRNA (n=8 mice per group). (E) Heart cross sections were co-immunostained with anti-CX43 and anti-ACTN2 antibodies. (F) CX43 protein level was evaluated via western blot analyses and (G) quantified using Image J software (n=8 mice per group). Mann-Whitney test.

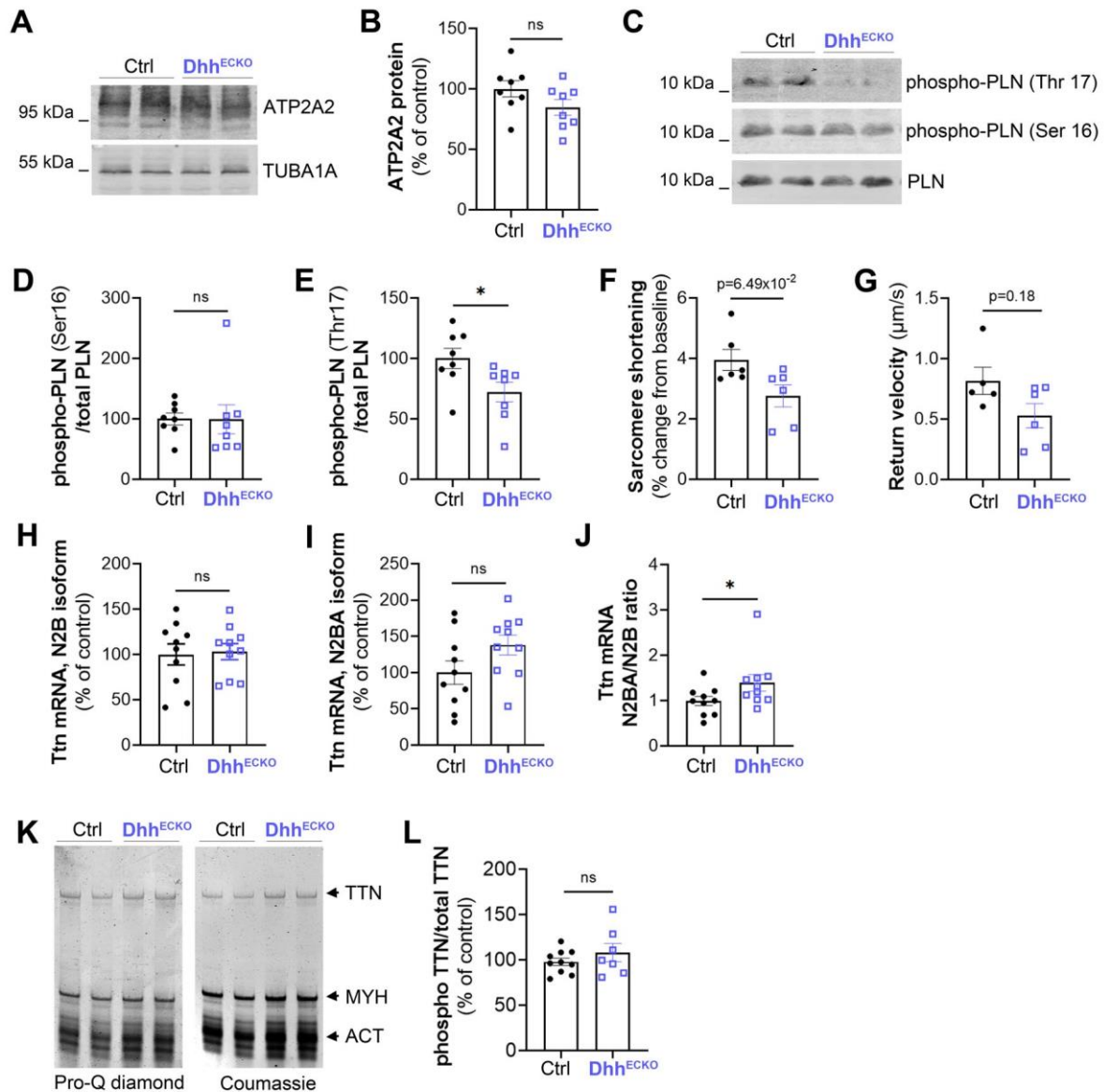


**Figure 4: *Dhh<sup>ECKO</sup>* mice display impaired cardiomyocyte relaxation.** *Cdh5-Cre/ERT2; Dhh<sup>Flox/Flox</sup>* (*Dhh<sup>ECKO</sup>*) mice and their control littermate (*Dhh<sup>Flox/Flox</sup>*) were administered with tamoxifen at 8 weeks of age and sacrificed at 12 weeks of age. (A) ATP2A2 protein level was evaluated via western blot analyses and (B) quantified using Image J software (n=8 mouse per group). (C) PLN phosphorylation was assessed by western blot analyses and (D-E) quantified using Image J software (n=8 mouse per group). (F-G) Ventricular cardiomyocyte were isolated. (F) Sarcomere shortening (bl% peak h.) was measured using a video-detection system (MyoCam, IonOptix) (n=7 and 6 mice per group). (G) Return velocity (Ret v) was measured using a video-detection system (MyoCam, IonOptix) (n=7 and 6 mice per group). (H) *Ttn* N2B and (I) *Ttn* N2BA mRNA were quantified by RT-qPCR in total heart extract and normalized to *Actb* mRNA (n=10 mice per group) and (J) the ratio N2BA over N2B was calculated. (K) Total heart proteins were separated on a 1% agarose gel and stained either with Pro-Q diamond to identify phosphoproteins or coumassie blue stain to identify total protein. (L) The ratio of phosphorylated TTN over total TTN was quantified and calculated using image J software. Mann-Whitney test.



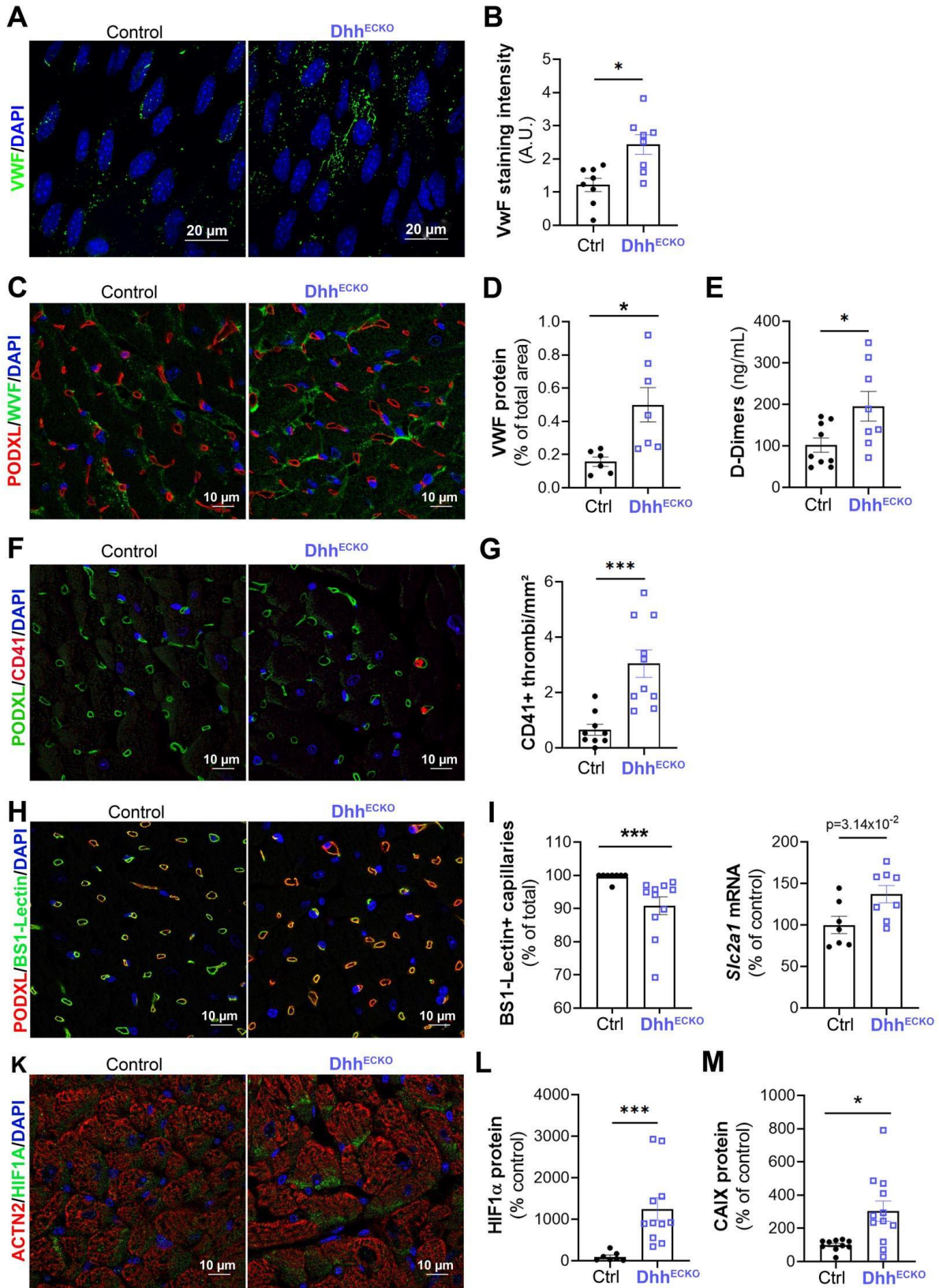


**Figure 5: The endothelium of *Dhh*<sup>ECKO</sup> mice is prothrombotic.** *Cdh5-Cre/ERT2; Dhh*<sup>Flox/Flox</sup> (*Dhh*<sup>ECKO</sup>) mice and their control littermate (*Dhh*<sup>Flox/Flox</sup>) were administered with tamoxifen at 8 weeks of age and sacrificed at 12 weeks of age. (A) Not permeabilized en face aortas were immunostained with anti-VWF antibodies. (B) Extracellular VWF was quantified using image J software (n=8 mice per group). (C) Heart cross sections were co-immunostained with anti-VWF antibody and anti-PODXL antibodies to identify capillaries. (D) Extravascular VWF staining was quantified using image J software (n=7 and 6 mice per group). (E) Circulating D-dimers were quantified via ELISA (n=8 mice per group). (F) Heart cross sections were co-immunostained with anti-CD41 antibodies to identify platelets and anti-Podocalyxin Like (PODXL) antibodies to identify capillaries. (G) The number of CD41+ thrombi per mm<sup>2</sup> was quantified using image J software (n=9 mice per group). (H-I) Mice were administered intravenously with FITC labelled BS1 lectin 2 minutes before sacrifice. (H) Heart cross sections were co-immunostained with anti-PODXL antibodies to identify total capillaries. (I) The percentage of capillaries perfused with BS1-lectin was quantified using image J software (n=9 mice per group). (J) *Slc2a1* mRNA expression was quantified via RT-qPCR and normalized to *Actb* mRNA expression (n=8 and 7 mice per group). (K) Heart cross sections were co-immunostained with anti-HIF1A antibodies to identify hypoxia and anti-ACTN2 antibodies to identify cardiomyocytes. (L) HIF1A protein level was quantified using image J software (n=10 mice per group). (M) Heart cross sections were immunostained with anti-CA9 antibodies to identify hypoxia. CA9 protein level was quantified using image J software (n=10 mice per group). Mann-Whitney test.

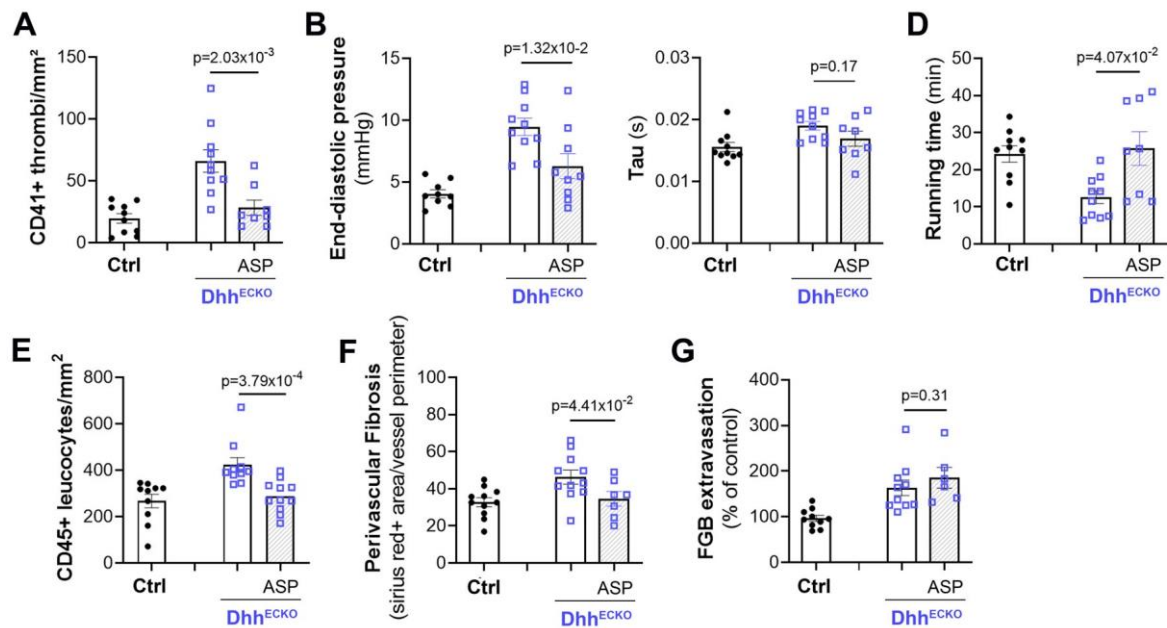


**Figure 6: Aspirin prevents the development of diastolic dysfunction in *Dhh*<sup>ECKO</sup> mice.** *Cdh5*-*Cre*/*ERT2*; *Dhh*<sup>Flox/Flox</sup> (*Dhh*<sup>ECKO</sup>) mice and their control littermate (*Dhh*<sup>Flox/Flox</sup>) were administered with tamoxifen at 8 weeks of age and treated or not with aspirin for 28 days. Mice were sacrificed at 12 weeks of age. **(A)** Heart cross sections were co-immunostained with anti-CD41 antibodies to identify platelets and anti- Podocalyxin Like (PODXL) antibodies to identify capillaries. The number of CD41+ thrombi per mm<sup>2</sup> was quantified using image J software (n=9 mice per group). **(B)** LV end diastolic pressure (EDP) was measured by left ventricular catheterization (n=9 mice per group). **(C)** Tau was measured by left ventricular catheterization (n=8 mice per group). **(D)** Running time was assessed on treadmill (n=4 and 9 mice per group). **(E)** Heart cross sections were immunostained with anti-CD45 antibodies to identify leucocytes. The number of CD45+ leucocytes per mm<sup>2</sup> was quantified using image J software (n=9 mice per group). **(F)** Heart cross sections were stained Sirius red to identify fibrosis. Perivascular red staining was quantified using image J software (n=7 and 9 mice per group). **(G)** Heart cross sections were immunostained with anti-FGB antibodies. FGB extravasation was quantified using image J software (n=6 and 9 mice per group). Mann-Whitney test.

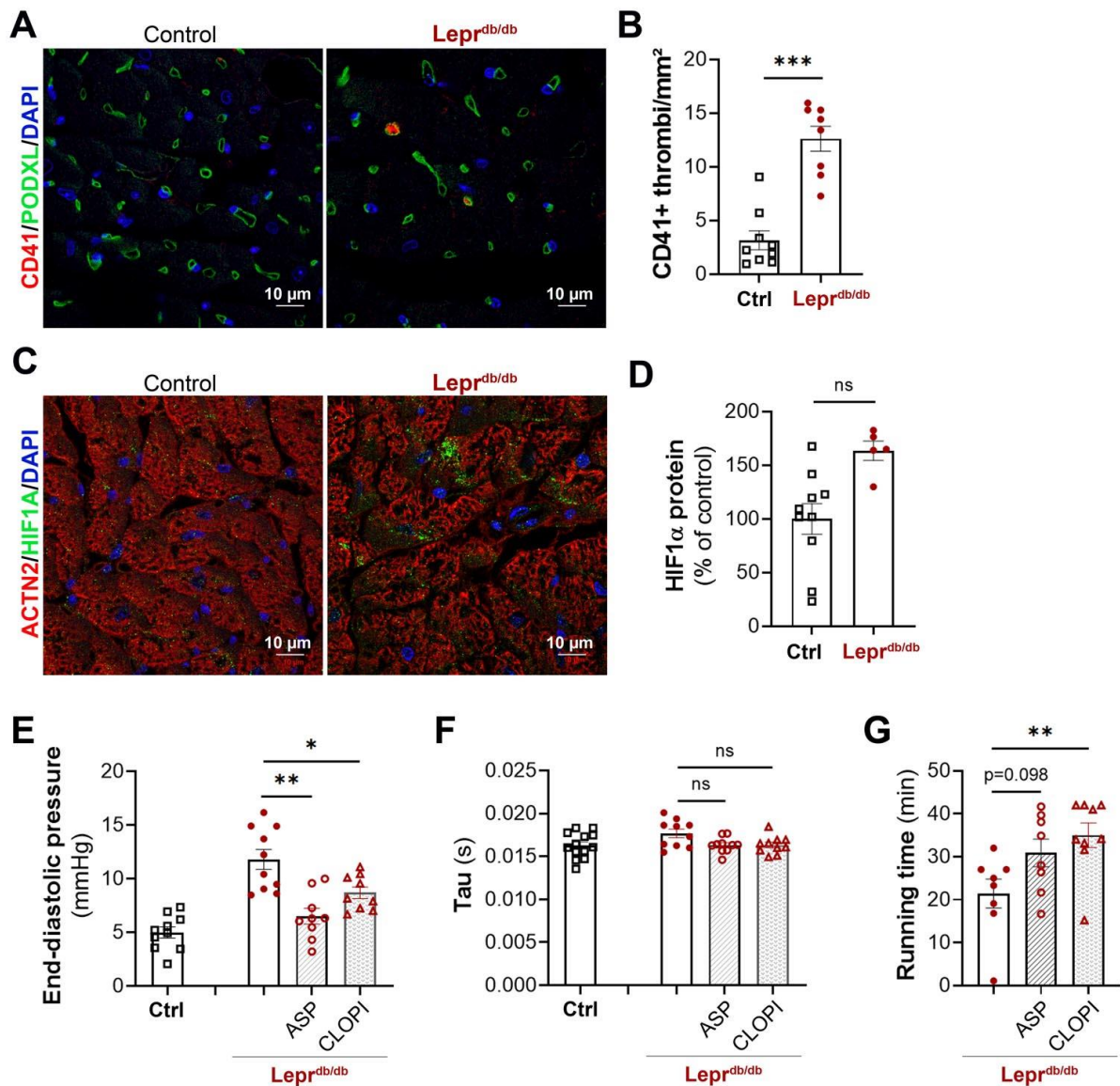


**Figure 7: Aspirin and clopidogrel prevent the development of diastolic dysfunction in *Lepr<sup>db/db</sup>* mice.** (A-D) *Lepr<sup>db/db</sup>* female mice and their control (*Lepr<sup>db/+</sup>*) littermate were sacrificed at 3 months of age. (A) Heart cross sections were co-immunostained with anti-CD41 antibodies to identify platelets and anti-PODXL antibodies to identify capillaries. (B) The number of CD41+ thrombi per mm<sup>2</sup> was quantified using image J software (n=8 mice per group). (C) Heart cross sections were co-immunostained with anti-HIF1A antibodies to identify hypoxia and anti-ACTN2 antibodies to identify cardiomyocytes. (D) HIF1A protein level was quantified using image J software (n=5 and 10 mice per group). (E-G) 8 week old *Lepr<sup>db/db</sup>* female mice and their control (*Lepr<sup>db/+</sup>*) littermate were treated or not with aspirin or clopidogrel. (E) LV end diastolic pressure (EDP) was measured by left ventricular catheterization (n=9 mice per group). (F) Tau was measured by left ventricular catheterization (n=9 mice per group). (G) Running time was assessed on treadmill (n= 9 mice per group). (B, D) Mann-Whitney test); (E-H) Kruskal-Wallis test with Bonferroni post-hoc.